

Different manipulation mode analysis of a radial symmetrical hexapod robot with leg–arm integration

Yi ZHENG, Kun XU (✉), Yaobin TIAN, Xilun DING

School of Mechanical Engineering and Automation, Beihang University, Beijing 100191, China

✉ Corresponding author. E-mail: xk_sea@163.com (Kun XU)

© The Author(s) 2022. This article is published with open access at link.springer.com and journal.hep.com.cn

ABSTRACT With the widespread application of legged robot in various fields, the demand for a robot with high locomotion and manipulation ability is increasing. Adding an extra arm is a useful but general method for a legged robot to obtain manipulation ability. Hence, this paper proposes a novel hexapod robot with two integrated leg–arm limbs that obtain dexterous manipulation functions besides locomotion ability without adding an extra arm. The manipulation modes can be divided into coordinated manipulation condition and single-limb manipulation condition. The former condition mainly includes fixed coordinated clamping case and fixed coordinated shearing case. For the fixed coordinated clamping case, the degrees of freedom (DOFs) analysis of equivalent parallel mechanism by using screw theory and the constraint equation of two integrated limbs are established. For the fixed coordinated shearing case, the coordinated working space is determined, and an ideal coordinated manipulation ball is presented to guide the coordinated shearing task. In addition, the constraint analysis of two adjacent integrated limbs is performed. Then, mobile manipulation with one integrated leg–arm limb while using pentapod gait is discussed as the single-limb manipulation condition, including gait switching analysis between hexapod gait and pentapod gait, different pentapod gaits analysis, and a complex six-DOF manipulation while walking. Corresponding experiments are implemented, including clamping tasks with two integrated limbs, coordinated shearing task by using two integrated limbs, and mobile manipulation with pentapod gait. This robot provides a new approach to building a multifunctional locomotion platform.

KEYWORDS leg–arm integration, hexapod robot, fixed coordinated manipulation, mobile manipulation

1 Introduction

In the natural world, the function of limbs of animals is not only locomotion but also manipulation. For example, among mammals, the primate is the representative animal. Their main mobility relies on the rhythmic motion of four limbs, and this species can realize manipulation by using their two forelimbs. Among insects, the ant moves with six limbs and carries objects with the first pair of legs [1]. Therefore, legged animals in nature provide a satisfactory template for the design of the legged robot to realize locomotion and manipulation functions. Hence, the leg–arm integration mechanism, which is presented and developed by Koyachi et al. [2], Takahashi et al. [3], and Mae et al. [4], has been applied in legged robots. This kind of mechanism can enable the legged robots to realize manipulation function without adding an extra arm and

utilize the degree of freedom (DOF) of the leg to replace the DOF of the arm. Japanese researchers developed TITAN robots [5–9], and TITAN-IX [10] is the outstanding prototype in this series. TITAN-IX is a quadruped robot, and one of its limbs is fixed with an end-effector. TITAN-IX can handle various tasks by utilizing this limb, and this limb becomes involved in the walking movement. Takubo et al. [11], the researchers of Osaka University, Japan, developed a hexapod robot, Asterisk. Its two legs can serve as arms to clamp the object while the remaining legs support the body. Several other research topics such as energy consumption optimization [12] and path planning [13,14] make the legged robots move smoothly and more intelligently.

However, adding an extra effector is still the major approach of realizing legged robot manipulation function [15–17]. For instance, the SpotMini robot [18,19] developed by Boston Dynamics is a representative prototype. The total DOF of the robot is 17, and the arm mounted on

the body possesses five DOFs. This arm can function as manipulator and support the body when the robot falls. In addition, these previous manipulation studies of the leg–arm integration mechanism simply focused on the additional function of the leg with/without an end-effector. Few researchers consider the switch flexibility of the limb between the leg and the arm. The research of complex coordinated manipulation by using multilimb robot is not sufficient either, for example, no other manipulation functions exist other than the simple clamping manipulation with two adjacent legs [20,21]. Therefore, a novel leg–arm integration mechanism design with high efficiency, flexibility, and multifunction can be considered an urgent research topic for legged robot manipulation.

In addition to locomotion and manipulation with “fixed” robot (in this paper, “fixed” means that the robot is still, and no gait exists), mobile manipulation (manipulating while moving, not manipulating after moving) is a valuable research topic that can improve the motion flexibility of the legged robot. However, in recent years, many researchers only pay attention to the mobile manipulator constituted by a wheel pedestal and a two- or three-DOF arm. Most researchers [22–25] focus on the controller of nonholonomic system because of the nonholonomic character for the vehicle robot. Most topics consider the adaptive robust force/motion control for mobile manipulators under holonomic and nonholonomic constraints in the presence of uncertainties and disturbances. Few researchers consider the mobile manipulation function of the legged robot. In addition, mobile manipulation cannot be achieved on most quadruped robots with leg–arm integration because for the quadruped robot with leg–arm integration, achieving a static stable gait is difficult while one integrated limb of the robot works as an arm. However, for the hexapod robot with leg–arm integration, mobile manipulation with stable static gait can be realized.

Therefore, the hexapod robot is an ideal prototype for locomotion, complex coordinated manipulation, and mobile manipulation. In this paper, a novel hexapod robot with two integrated leg–arm limbs is developed. Based on this robot, the robot structure design is introduced in Section 2. Kinematic analyses under different fixed coordinated manipulation cases are discussed in Section 3. Mobile manipulation with one integrated leg–arm limb is discussed in Section 4. The different manipulation functions of the novel robot presented in Sections 3 and 4 are validated by experiments in Section 5. This paper is concluded in Section 6.

2 Design of integrated leg–arm robot

According to the different geometrical shape of the robot body, the typical hexapod robot can be divided into

bilateral symmetrical rectangular body [26,27] and radial symmetrical hexagonal body [28]. Owing to the better turning ability and static stability [29], the radial symmetrical hexagonal body is applied in this paper. The robot body can be considered a mobile platform, and six limbs are serial branches, which are evenly distributed on the mobile platform.

In general, the normal hexapod robot leg is designed with three joints; hence, the normal leg of this novel robot obtains three joints. With regard to the integrated leg–arm limb, the similarity of manipulation realization between the robot arm and the integrated leg–arm limb is considered; hence, the design idea of robot arm can be used for reference. Moreover, the human arm is an excellent template for robot arm design, and the physiological structure of the human arm is discussed first. Figure 1(a) shows that the human arm is mainly composed of shoulder joint, humerus, elbow joint, ulna, radius, and wrist joint. The movement of the arm relies on the activities of these three joints. Figure 1(b) shows that every arm owns seven DOFs without considering the DOF of the fingers. With regard to the distribution of these seven DOFs, bionic research has two main views: Rosheim [30] presented that the shoulder joint obtained three DOFs, the elbow joint obtained one, and the wrist joint obtained three; otherwise, Fang [31] considered that the three mentioned joints obtained three, two, and two DOFs. In general, the previous theory is accepted to guide the mechanism design of robot arm. Hence, this structure of a seven-DOF robot arm can be equivalent to a spherical-joint revolute-joint spherical-joint mechanism. In this paper, the number of joints is simplified to five because this limb design is based on a legged robot, not a fixed base or a vehicle, and excessively redundant DOF is unnecessary. Finally, Fig. 2 shows the whole robot mechanism sketch.

In Fig. 2, Limbs 1 and 2 are designed as integrated leg–arm limbs with five DOFs; Legs 3–6 are normal legs with three rotating joints. Two main coordinate systems are built here: $\{O_g\}$ is the global coordinate system fixed on the ground, and $\{COB\}$ (center of body) is the moving coordinate system fixed on the center of robot body mass. R_b is the radius of the robot body.

Figure 3(a) shows the mechanism sketch of the four normal legs. It has three links. These three parts are named hip, thigh, and shank. They are connected by Joints 2 and 3. The coordinate system of the normal leg at the first joint is denoted as $\{O_i\}$ ($i = 3, 4, 5, 6$). The lengths of hip, thigh, and shank are denoted as l_m ($m = 1, 2, 3$). The rotation angle of every joint is θ_{ij} ($i = 3, 4, 5, 6; j = 1, 2, 3$).

Figure 3(b) shows the mechanism sketch of the two integrated leg–arm limbs. It has six links that are denoted as hip, thigh, Shank 1, Shank 2, Arm 1, and Arm 2. The arm is composed of Joint 4, Arm 1, Joint 5, Arm 2, and end-effector. These special integrated limbs have five

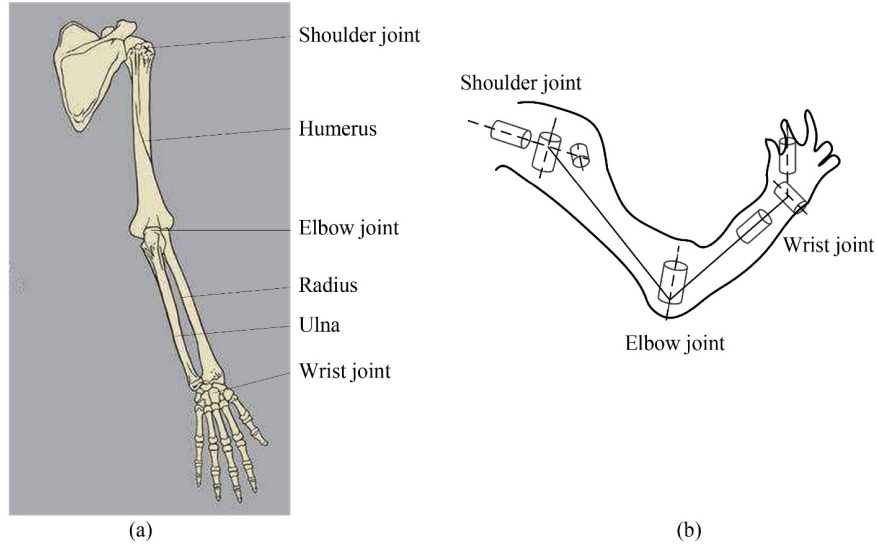


Fig. 1 Skeleton and seven main joints of human arm: (a) skeletal structure of human arm, (b) main equivalent joints in human arm.

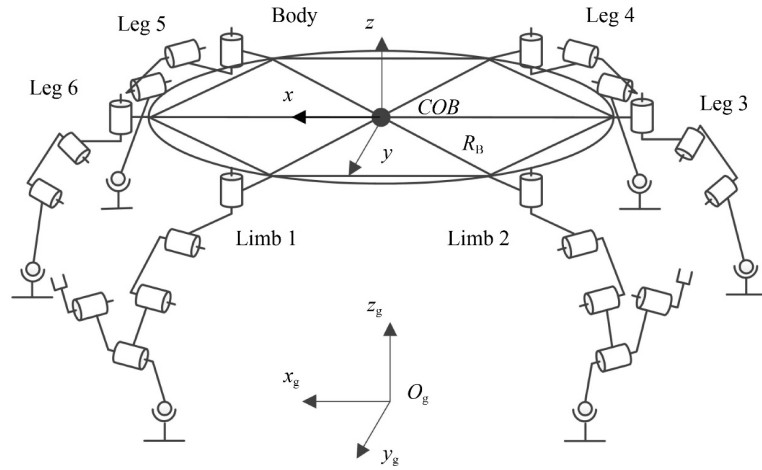


Fig. 2 Structural sketch of novel hexapod robot.

joints and one end-effector. The coordinate system of this limb at the first joint is denoted as $\{O_i\}$ ($i = 1, 2$). The length of each link is denoted as l_m ($m = 1, 2, 4, 5$) and l_{3k} ($k = 1, 2$). The hip and thigh lengths of the integrated leg–arm limbs are equal to those of the normal ones. The length of Shanks 1 and 2 should satisfy the following equation: $l_3 = l_{31} + l_{32}$. Moreover, the lengths of Arms 1 and 2 satisfy $l_4 + l_5 \leq l_{31}$. The rotation angle of every joint is θ_{ij} ($i = 1, 2; j = 1, 2, \dots, 5$). To describe robot performance conveniently, the main dimensions of the robot are given in Table 1.

Considering the manipulated object weight, a positive y -axis ($\{COB\}$) offset of robot gravity center exists and may cause the balance loss or even overthrow. Hence, the proper distribution of components on the robot body is necessary. The distribution of components (battery, slave computer) can be set with a negative y -axis offset to balance the positive y -axis offset. As a result, the moment

generated by the manipulated object can be balanced. According to the mechanism design, the 3D model of the robot is built in SolidWorks 2012, as shown in Fig. 4(a) and the physical prototype of the robot is constructed, as shown in Fig. 4(b). The major components of the prototype are listed in Table 2.

Figure 5(a) shows the detailed structure of the normal leg. Compared with the normal legs, the integrated limbs obtain five DOFs. The integrated leg–arm limbs can achieve swinging and supporting functions as normal legs when the parts of the arm are folded into Shank 1, as shown in Fig. 5(b). In Fig. 5(c), the arm stretches out, and Shank 2 is withdrawn into Shank 1. Hence, the integrated leg–arm limbs can realize locomotion function as leg and manipulation functions as arm. The novel robot can achieve different manipulating tasks due to the various forms of the end-effectors installed on the tip of the integrated limbs.

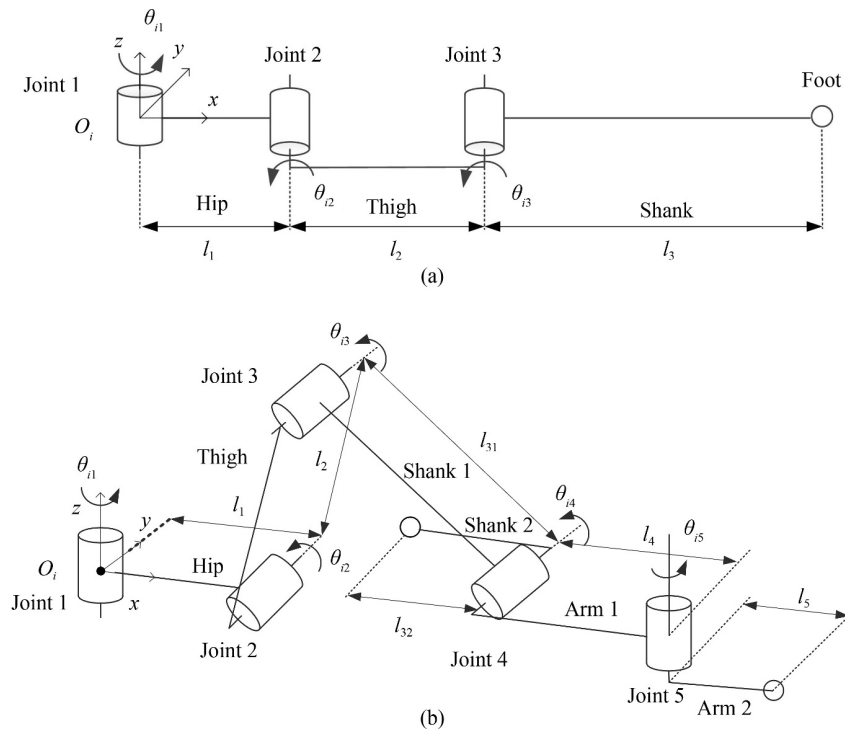


Fig. 3 Mechanism sketch of robot limbs: (a) normal leg structural sketch, (b) integrated leg–arm limb structural sketch.

3 Fixed coordinated manipulation with two integrated leg–arm limbs

During manipulation mode, the arm part of the integrated leg–arm limb is extended outward by the rotation of Joint 4. Based on the number of integrated leg–arm limbs involved in manipulation, the novel robot can achieve manipulation mode by one integrated leg–arm limb or two integrated leg–arm limbs. In this section, the fixed coordinated manipulation with two adjacent integrated leg–arm limbs is presented first. Although the cases of fixed two-limb coordinated manipulation are various, these cases can be classified as tight coordinated

Table 1 Main geometric parameters of robot

Parameter	Symbol	Length/mm
Hip	l_1	65
Thigh	l_2	120
Shank	l_3	270
Shank 1	l_{31}	200
Shank 2	l_{32}	70
Arm 1	l_4	25
Arm 2	l_5	105
Radius of body	R_B	200

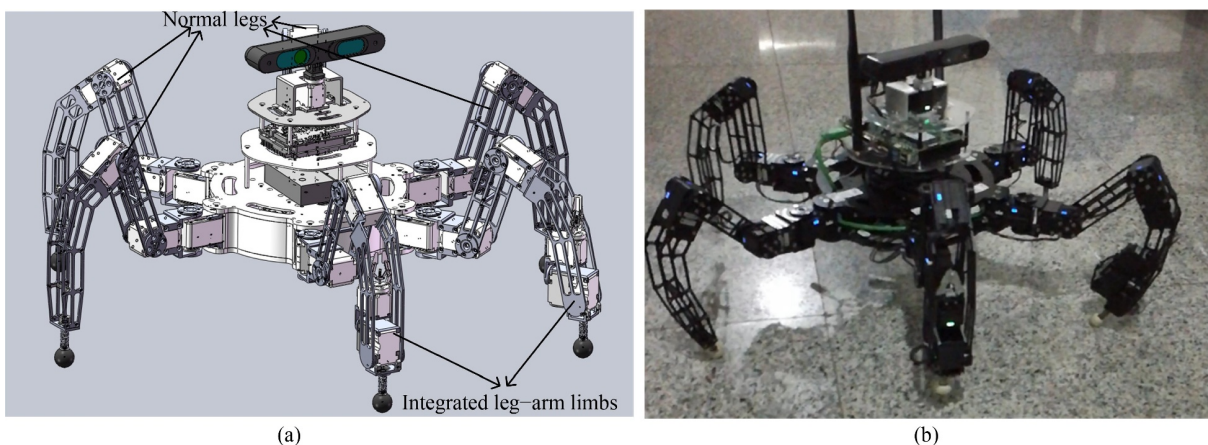
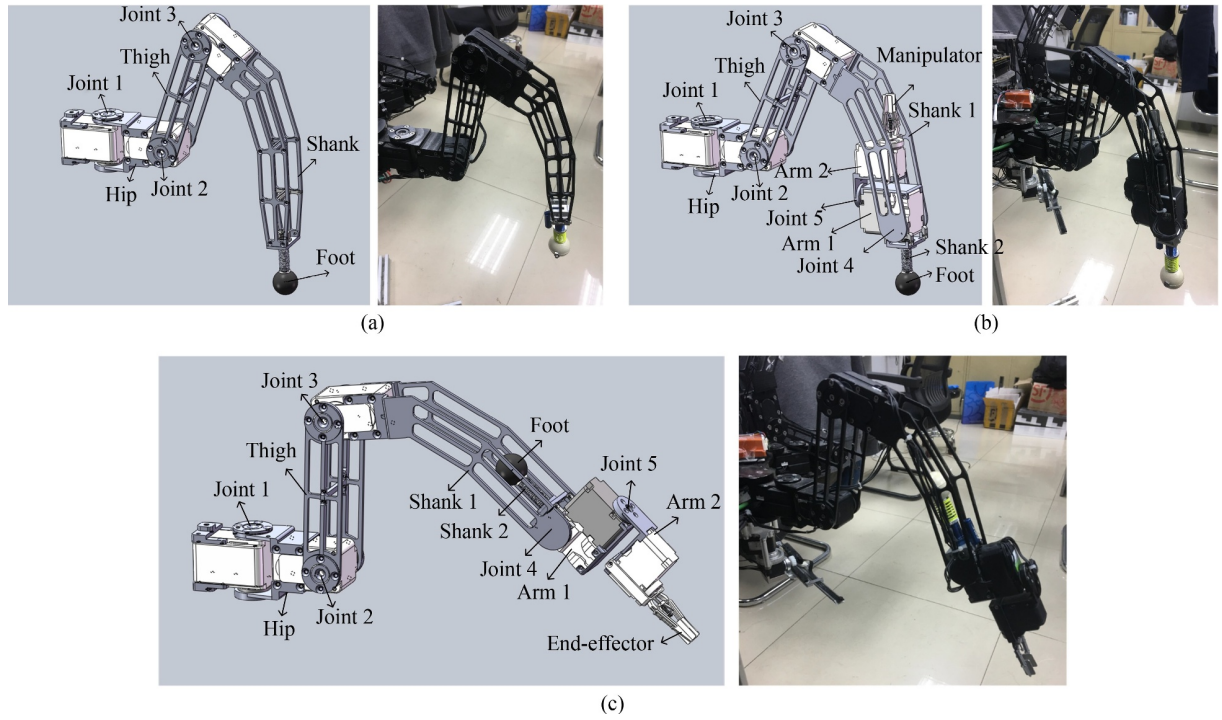


Fig. 4 Overall concrete structure of novel robot: (a) 3D virtual model of robot, (b) physical prototype of robot.

Table 2 Major components of robot prototype

Component	Number	Notes (material/type)	Weight/kg
Upper chassis (body)	1	2024-T4/not applicable	0.393
Under chassis (body)	1	2024-T4/not applicable	0.377
Normal limbs	4	2024-T4/not applicable	0.667
Integrated limbs	2	2024-T4/not applicable	0.862
Driving servo (limb)	18	Not applicable/Herkulex DSR-0401	0.123
Driving servo (manipulator)	6	Not applicable/Herkulex DSR-0101	0.045
Camera	1	Not applicable/ASUS XtionPROLIVE	0.450
Slave computer	2	Not applicable/Advantech MIO-2261N	0.420
IMU	1	Not applicable/XSENS MTI-100	0.055

**Fig. 5** Comparison diagrams of 3D virtual robot model and physical robot prototype: (a) detailed structure of normal leg, (b) walking status of integrated leg–arm limb, and (c) manipulation status of integrated leg–arm limb.

manipulation and loose coordinated manipulation in general. Moreover, coordinated clamping manipulation and coordinated shearing manipulation are two representative manipulation cases of these two manipulations. Hence, these two cases are selected for analysis in this paper.

3.1 Coordinated clamping manipulation with two adjacent integrated limbs

Figure 6 shows that the robot can obtain the function of fixed coordinated clamping object by using two adjacent integrated limbs. Considering the robot status, when the robot manipulates the object using two adjacent integrated limbs, the four remaining legs support and stabilize the robot body. $\{O\}$ is the object coordinate

system set on the geometric center of the object. Coordinate system $\{O_i\}$ ($i = 3, 4, 5, 6$) is set on Joint 1 of the supporting leg, and coordinate system $\{O_i\}$ ($i = 1, 2$) is set on Joint 1 of the integrated limb. Coordinate system $\{p_i\}$ ($i = 3, 4, 5, 6$) is set on the end of the supporting leg foot.

When the robot utilizes two adjacent integrated limbs, the robot should satisfy the condition of grasping force closure [32] to ensure clamping stability. The static friction coefficient between limb end and object is assumed to be μ ($\mu \in [1, 4]$), and the material of end-effector finger is rubber. Therefore, when the robot executes the clamping task with two adjacent integrated limbs, the soft finger contact model is applied, as shown in Fig. 7.

This case assumes that the geometric center of the

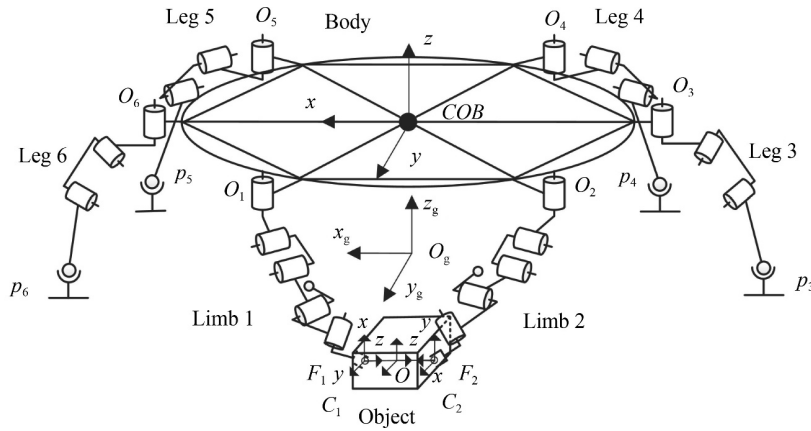


Fig. 6 Build of clamping coordinate system on hexapod robot.

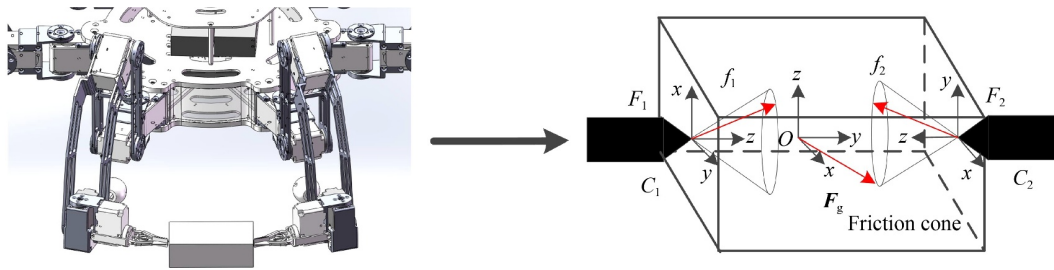


Fig. 7 Two soft finger clamping model of integrated leg-arm limbs.

contact surface is the clamped point of the object, and the position of the clamped points remains fixed. Therefore, no relative movement exists between the object and the limb end during clamping. Coordinate system $\{F_i\}$ is fixed on the end-effector end of the limb and located at the clamped point. Coordinate system $\{C_i\}$ is fixed on the object and located at the clamped point. To maintain the stability of the whole clamping system during the manipulating process, the component force along the z -axis ($\{C_i\}$) f_{iz} effected on the object of each limb end should satisfy the following constraint condition:

$$\begin{cases} \mu^2 f_{iz}^2 \geq \frac{F_{gx}^2}{4} + \frac{F_{gz}^2}{4}, & \text{if } F_{gy} < 0, \\ \mu^2 f_{iz}^2 \geq \frac{F_{gx}^2}{4} + \frac{F_{gz}^2}{4}, & \text{if } F_{gy} \geq 0, \end{cases} \quad (1)$$

where F_{gx} and F_{gy} are components of F_g on x - and y -axis, respectively, F_g is the gravity of the object.

The legged robot structural sketch under clamping task can be based on the physiology anatomy of the human arm shown in Fig. 1 because this task case is similar to anthropomorphic dual-arm robot. For the structure of this leg-arm robot, the single limb performs five DOFs, and the number of DOFs can be distributed as 2, 1, and 2. Thus, the robot body, two integrated limb branches, and the object can be regarded as a parallel mechanism (PM). Owing to the various clamping states of the moving platform (object), a representative stable clamping state is

introduced and analyzed in this paper (Figure 6 shows two platforms are parallel; the equivalent mechanism under this state is shown in Fig. 8, and the revolution axes of Joints 1 and 5 are parallel).

The DOF of a parallel mechanism can be calculated by the modified Grübler-Kutzbach criterion [33]:

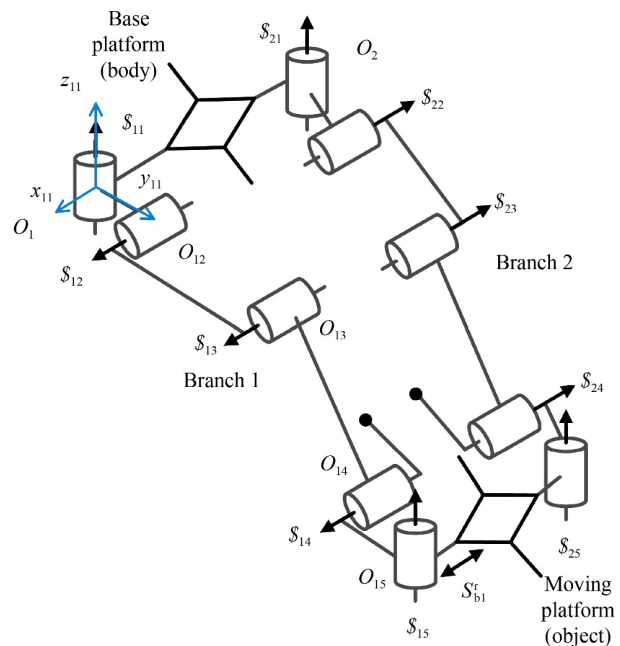


Fig. 8 Equivalent parallel mechanism of robot and object.

$$df = d(n - k - 1) + \sum_{i=1}^k \varphi_i + \varepsilon - \zeta, \quad (2)$$

where $d = 6 - \lambda$ is called the order of the mechanism, λ is the number of independent common constraints in the mechanism, n is the total number of links, k is the number of kinematic pairs, φ_i is the DOF of the i th kinematic pair, ε represents the number of virtual constraints (the redundant constraints that remove the common constraints), and ζ is the passive DOF.

Clearly, the number passive DOFs of the PM is 0. Then, the twist system analysis of two branches can be determined in this instantaneous configuration as follows:

$$\mathbf{S}_{\text{br1}} = \begin{cases} \mathcal{S}_{11} = (0 \ 0 \ 1; 0 \ 0 \ 0), \\ \mathcal{S}_{12} = (1 \ 0 \ 0; 0 \ 0 \ -y_{o_{12}}), \\ \mathcal{S}_{13} = (1 \ 0 \ 0; 0 \ z_{o_{13}} \ -y_{o_{13}}), \\ \mathcal{S}_{14} = (1 \ 0 \ 0; 0 \ z_{o_{14}} \ -y_{o_{14}}), \\ \mathcal{S}_{15} = (0 \ 0 \ 1; y_{o_{15}} \ 0 \ 0), \end{cases}$$

$$\mathbf{S}_{\text{br2}} = \begin{cases} \mathcal{S}_{21} = (0 \ 0 \ 1; 0 \ -x_{o_2} \ 0), \\ \mathcal{S}_{22} = (1 \ 0 \ 0; 0 \ 0 \ -y_{o_{22}}), \\ \mathcal{S}_{23} = (1 \ 0 \ 0; 0 \ z_{o_{23}} \ -y_{o_{23}}), \\ \mathcal{S}_{24} = (1 \ 0 \ 0; 0 \ z_{o_{24}} \ -y_{o_{24}}), \\ \mathcal{S}_{25} = (0 \ 0 \ 1; y_{o_{25}} \ -x_{o_{25}} \ 0). \end{cases} \quad (3)$$

The constrained wrench systems of the two branches are $\mathbf{S}_{\text{br1}}^r = \mathbf{S}_{\text{br2}}^r = (0 \ 0 \ 0; 0 \ 1 \ 0)$ based on $\mathbf{S}_{\text{br1}} \Delta \mathbf{S}_{\text{br1}}^r = \mathbf{0}$, and the generated constraint on the moving platform is couple. Considering that the two platforms are parallel and the two constraint couples are parallel, coplanar, dependent ($\mathbf{S}_{\text{br1}}^r // \mathbf{S}_{\text{br2}}^r$), in this instantaneous configuration, two rotation freedoms are perpendicular to the direction of the constraint couple.

The constrained wrench set of the moving platform is $\langle \mathbf{S}^r \rangle = \mathbf{S}_{\text{br1}}^r \uplus \mathbf{S}_{\text{br2}}^r$; hence, the number of elements in set $\langle \mathbf{S}^r \rangle$ is $\text{card}(\langle \mathbf{S}^r \rangle) = 2$. Then, the number of redundant constraints can be determined:

$$c = \text{card}(\langle \mathbf{S}^r \rangle) - \dim(\mathbf{S}^r) = 1. \quad (4)$$

The twist system of the PM is $\mathbf{S}_m = \mathbf{S}_{\text{br1}} \cup \mathbf{S}_{\text{br2}}$. Then, based on $\mathbf{S}_m \Delta \mathbf{S}^c = \mathbf{0}$, the constrained wrench system of the PM is as follows:

$$\mathbf{S}^c = (0 \ 0 \ 0; 0 \ 1 \ 0). \quad (5)$$

The number of common constraints λ is 1 due to $\lambda = \dim(\mathbf{S}^c)$, then $d = 6 - \lambda = 5$.

For the number of virtual constraints, ε can be computed as follows:

$$\varepsilon = c - (\rho - 1)(6 - d) = 0, \quad (6)$$

where ρ presents the number of branches, and $\rho = 2$.

Hence, $d = 5$, $n = 10$, $k = 10$, $\sum_{i=1}^k \varphi_i = 10$, $\varepsilon = 0$, and $\zeta = 0$. The DOF of the PM is calculated as follows:

$$df = 5 \times (10 - 10 - 1) + 10 = 5. \quad (7)$$

The DOF result shows that this equivalent PM is an

insufficient DOF system. Figure 6 shows that the robot performs the coordinated clamping task by using two adjacent limbs. The supporting legs of the robot can adjust the angles of the joints to compensate for the one remaining DOF.

In the case of stable clamping, the motion constraint analysis of two integrated limbs is important as well. Figure 9 shows that normalized base $\{o \mathbf{e}_j^o\}$ ($j = 1, 2, 3$) is fixed in the center of mass (COM) of the object, and normalized bases $\{o_i \mathbf{e}_j^o\}$ ($i = 1, 2; j = 1, 2, 3$) are fixed in the centers of the rotating hinges.

The relative position and the orientation between the integrated limbs are assumed to remain unchanged. Thus,

$$\mathbf{P}_{o_1 o} = \mathbf{P}_{o_1 o_2} + \mathbf{P}_{o_2 o} = \mathbf{P}_{o_1 o_2} + \mathbf{P}_{o_2 o_{25}} + \mathbf{P}_{o_{25} o}, \quad (8)$$

$${}^{o_1} \mathbf{R} {}^{o_{15}} \mathbf{R} = {}^{o_1} \mathbf{R} {}^{o_2} \mathbf{R} {}^{o_{25}} \mathbf{R}. \quad (9)$$

Equations (8) and (9) are constraint equations of the position and the orientation of two limbs. Hence, the constraint equations of their projection in base $\{o_1 \mathbf{e}_j^o\}$ are as follows:

$$\mathbf{P}_{o_1 o}^{o_1} + {}^{o_1} \mathbf{R} \mathbf{P}_{o_{15} o}^{o_{15}} = \mathbf{P}_{o_1 o_2}^{o_1} + {}^{o_1} \mathbf{R} \mathbf{P}_{o_2 o_{25}}^{o_2} + {}^{o_1} \mathbf{R} {}^{o_2} \mathbf{R} \mathbf{P}_{o_{25} o}^{o_{25}}, \quad (10)$$

$${}^{o_1} \mathbf{R} {}^{o_{15}} \mathbf{R} {}^{o_{15} o} \mathbf{R} = \mathbf{I}, \quad (11)$$

where \mathbf{I} is a 3×3 unit matrix, and $\mathbf{P}_{o_{15} o}^{o_{15}}$, $\mathbf{P}_{o_1 o_2}^{o_1}$, $\mathbf{P}_{o_{25} o}^{o_{25}}$, ${}^{o_1} \mathbf{R}$, ${}^{o_{15}} \mathbf{R}$, and ${}^{o_2} \mathbf{R}$ are determined by given known conditions. If the orientation of the object and the COM (Point o) movement have been planned, then $\mathbf{P}_{o_1 o}^{o_1}$ and ${}^{o_1} \mathbf{R}$ are also known.

Thus, the constraint equations of Limb 1 are as follows:

$$\mathbf{P}_{o_1 o}^{o_1} = \mathbf{P}_{o_1 o_{15}}^{o_1} + {}^{o_1} \mathbf{R} \mathbf{P}_{o_{15} o}^{o_{15}}, \quad (12)$$

$${}^{o_1} \mathbf{R} = {}^{o_1} \mathbf{R} {}^{o_{15}} \mathbf{R}. \quad (13)$$

The constraint equations of Limb 2 are as follows:

$$\mathbf{P}_{o_1 o}^{o_1} = \mathbf{P}_{o_1 o_2}^{o_1} + {}^{o_1} \mathbf{R} \mathbf{P}_{o_2 o_{25}}^{o_2} + {}^{o_1} \mathbf{R} {}^{o_2} \mathbf{R} \mathbf{P}_{o_{25} o}^{o_{25}}, \quad (14)$$

$${}^{o_1} \mathbf{R} = {}^{o_1} \mathbf{R} {}^{o_2} \mathbf{R} {}^{o_{25}} \mathbf{R}. \quad (15)$$

${}^{o_1} \mathbf{R}$, ${}^{o_2} \mathbf{R}$, $\mathbf{P}_{o_1 o_{15}}^{o_1}$, and $\mathbf{P}_{o_2 o_{25}}^{o_2}$ can be determined from Eqs. (12)–(15). Hence, the position and the orientation of two integrated limbs are determined.

3.2 Coordinated shearing manipulation with two adjacent integrated limbs

Coordinated manipulation with two limbs is an important function of the robot. In this section, a fixed coordinated shearing manipulation task is designed and introduced.

To fulfill the fixed coordinated shearing manipulation task, the coordinated working space of the integrated limbs is discussed necessarily. According to the kinematic analysis of the single integrated limb, based on Table 1 and the rotation range of each joint (Table 3), the ‘‘Monte Carlo Method’’ [34] is applied to simulate the 3D working space of the single integrated limb. In addition, the two integrated leg–arm limbs can be divided into main limb

and slave limb. Figure 10 shows that the coordinated working space is the intersecting area of the main limb working space and the slave limb working space. Coordinated manipulation should be located in this area.

However, when the robot proceeds to the coordinated shearing task, the manipulation location cannot be simply

regarded as a point because during the process, the end-effectors of the two limbs do not coincide with each other, and the distance between the original points of the two end-effector coordinate systems exists. These two original points should also be included in the coordinated working space.

For simply describing the coordinated manipulation location, the concept of ideal coordinated manipulation ball is presented. A rigid rope is regarded as the object.

Figure 11 shows E_1 and E_2 are origins of $\{E_1\}$ and $\{E_2\}$, respectively; $\{E_1\}$ and $\{E_2\}$ are fixed in the connection points between end-effector and Arm 2 of the

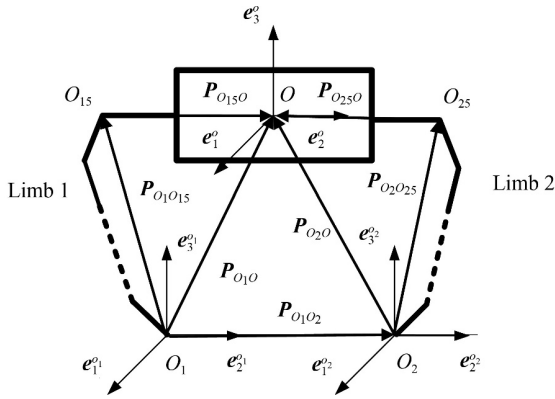


Fig. 9 Coordinated clamping case of hexapod robot.

Table 3 Joint rotation range of integrated leg–arm limb

Joint number	Symbol	Range/(°)
1	θ_{i1}	[0, 180]
2	θ_{i2}	[-60, 60]
3	θ_{i3}	[-30, 60]
4	θ_{i4}	[0, 180]
5	θ_{i5}	[0, 180]

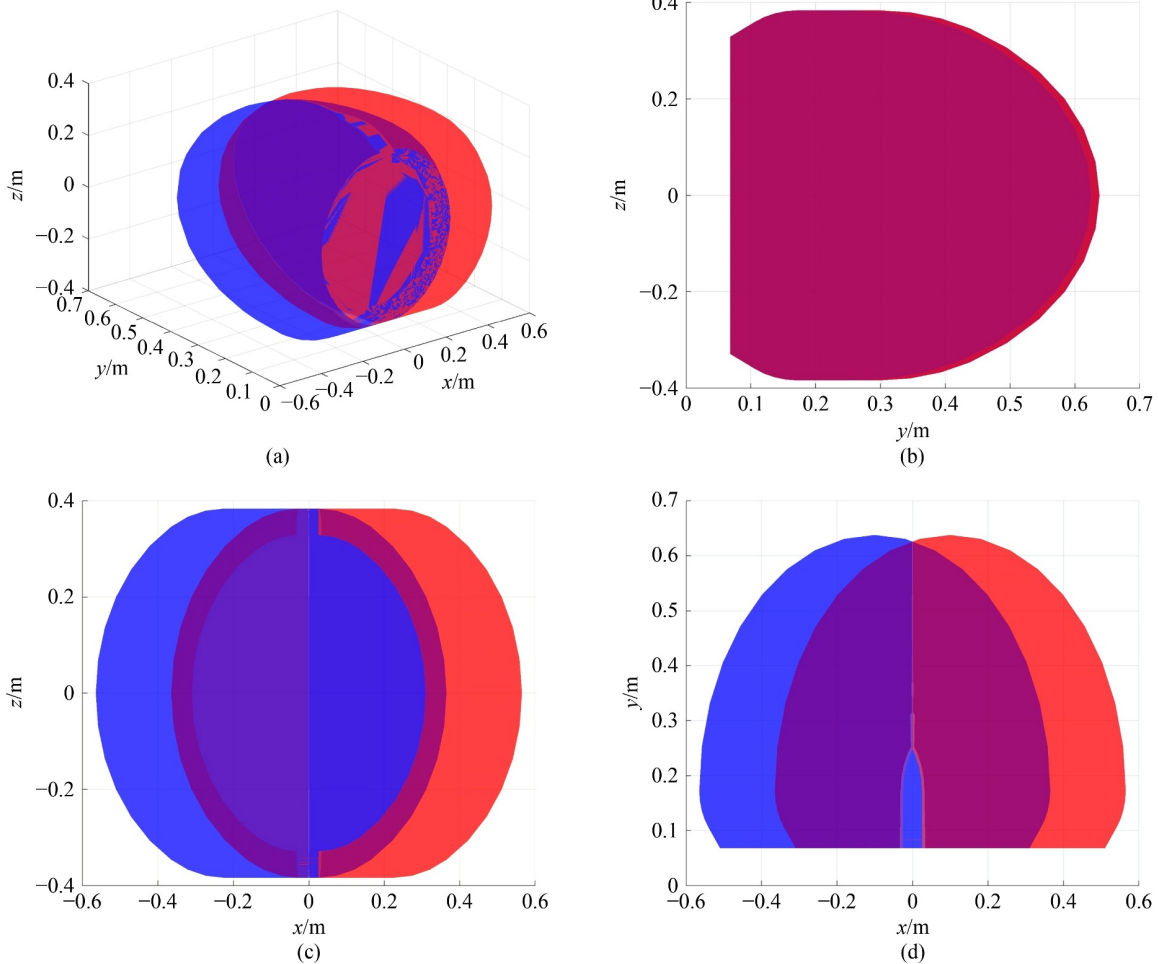


Fig. 10 Coordinated working space of two integrated leg–arm limbs: (a) 3D view of coordinated working space, (b) projection of coordinated working space in $y-z$ plane, (c) projection of coordinated working space in $x-z$ plane, and (d) projection of coordinated working space in $x-y$ plane.

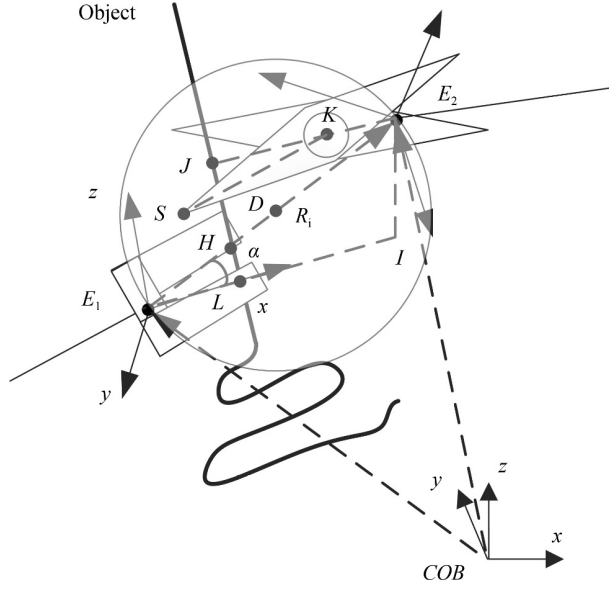


Fig. 11 Ideal coordinated manipulation ball of coordinated shearing manipulation.

main limb and the slave limb, respectively. In this paper, the straight line of E_1E_2 is assumed to intersect with the manipulated object (line). First, the position of E_1 in the coordinated working space is confirmed. Hence, the coordinates of E_1 in $\{COB\}$ are known as $(x_{E_1}^{COB}, y_{E_1}^{COB}, z_{E_1}^{COB})$. E_1L is vertical to the object and intersects the object at L . The length of E_1L is l_l . E_1E_2 intersects the object at H , and the angle between E_1E_2 and E_1L is α . E_2I is vertical to E_1L and intersects E_1L at I . K is the hinge joint point of the scissors. S is the end point on the scissors' head. E_2K is vertical to the object and intersects the object at J . The length of SK , JK , and KE_2 are l_s , l_j , and l_k , respectively (l_s and l_k are constants). Therefore, the length of JE_2 is $\{l_j + l_k\}$, and the range of $\{l_j + l_k\}$ is $[l_k, l_s + l_k]$. Hence, the diameter R_i of the ideal coordinated manipulation ball can be determined:

$$R_i = \frac{l_l + l_j + l_k}{\cos \alpha}. \quad (16)$$

The coordinates of E_2 in $\{E_1^M\}$ are $(R_i \cos \alpha, 0, R_i \sin \alpha)$.

If the robot could realize the coordinated shearing manipulation, the ball should be included in the coordinated working space. In addition, the boundary condition of this working case is that the ball and the internal surface of the coordinated working space are tangent.

Compared with the clamping case using two limbs, shearing manipulation case is a kind of loose coordination case. The constraint analysis of loose coordination case is necessary to program the integrated limb motion. [Figure 12](#) shows that the left limb serves as the main limb, and the other one serves as the slave limb. The manipulation parts move to the position, which is in the coordinated operation space. The main limb clamps the object, and the scissors of the slave limb approaches the object.

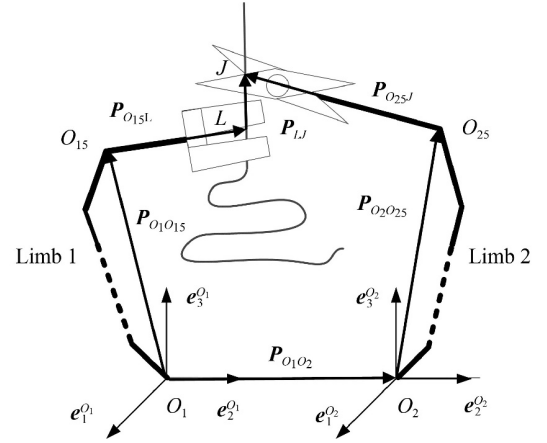


Fig. 12 Coordinated shearing case of hexapod robot.

The complete pose constraint is presented as follows:

$$P_{O_1O_{15}}^{O_1} + {}_{O_{15}}R_{O_{15}L}^{O_{15}} + {}_L R_{LJ}^L = P_{O_1O_2}^{O_1} + {}_{O_2}R_{O_2O_{25}}^{O_2} + {}_{O_{25}}R_{O_{25}J}^{O_{25}}, \quad (17)$$

$${}_{O_{15}}R_{L}^{O_{15}} R_{LJ}^L R_{O_{25}}^J R_{O_2}^{O_{25}} R_{O_1}^{O_2} = I. \quad (18)$$

Then, the fixed coordinated shearing task strategy can be decomposed into few parts, as shown in [Fig. 13](#). Based on this task strategy, a coordinated shearing experiment can be designed and carried out to verify the dexterous coordinated manipulation ability of the robot.

4 Mobile manipulation with one integrated leg–arm limb

Manipulating while moving is an effective way for an animal to increase efficiency and gain time. For the novel hexapod robot presented in this paper, due to the leg–arm integration mechanism and the high fault tolerance of the limbs, the robot can evidently achieve mobile manipulation function. Compared with the mobile manipulation of the wheel–track mobile robot with extra arms, this novel hexapod robot can realize mobile manipulation function without adding extra effectors or arms. This feature can save the space of the robot body and reduce the cost. Moreover, due to the specialty of the legged robot, this hexapod robot can be employed in several specific environments that are not fit for the wheel–track mobile robot, but the working speed of the wheel–track mobile robot is still higher.

The hexapod robot obtains various efficient walking gaits because the high redundancy of limb number. The hexapod gait is a representative gait that is deeply researched by scholars, and the 3+3 mixed gait [28] is employed in movement. However, the pentapod gait lacks sufficient research. In this section, the process that the hexapod robot continuously walks from the hexapod gait to the pentapod gait, and enters the mobile manipulation state while running the pentapod gait is

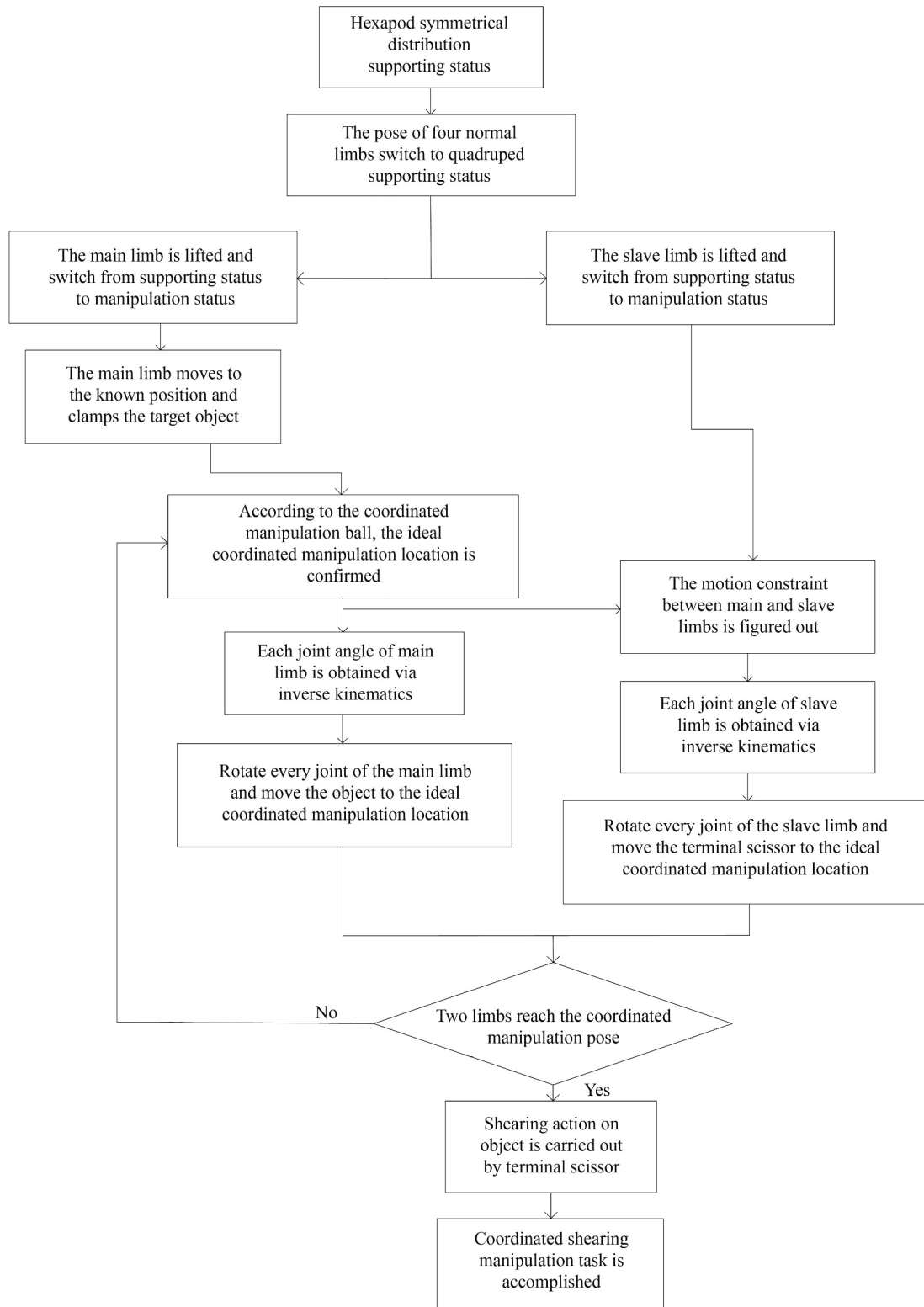


Fig. 13 Task strategy of coordinated shearing manipulation case.

introduced first. After the mobile manipulation, the hexapod robot continuously transitions from the pentapod gait to the hexapod gait. According to the characteristic of the radial symmetrical hexapod robot, the regular pentagon distribution of the footholds is designed for the

continuous omnidirectional pentapod gait. The stability and the velocity of the pentapod gait are lower than the hexapod gait for the radial symmetrical hexapod robot. At this expense, the integrated limb can completely become a serial manipulator with compensation.

4.1 Switch between hexapod gait and pentapod gait

To realize the continuous movement for mobile manipulation, the robot body also maintains translation during the switch between hexapod gait and pentapod gait.

The switch from hexapod gait to pentapod gait based on $\{COB\}$ is shown in Fig. 14. When the normal leg of the hexapod robot enters the stance state, the switch from hexapod gait to pentapod gait can start.

The trajectory and the footholds of the three swing limbs are changed and form a regular pentagon. When the integrated limb of the hexapod robot enters the stance state during the switching process, the stability of the robot is smaller than the hexapod gait. Then, the trajectory and the footholds of the left two swing normal legs change, and the integrated limb serves as an arm. During the switch from hexapod gait to pentapod gait, the robot has been walking, and the manipulation has been working.

After the mobile manipulation, the switch from pentapod gait to hexapod gait based on $\{COB\}$ is shown in Fig. 15. The switch from pentapod gait to hexapod gait starts when five limbs support the hexapod robot.

The trajectory and the footholds of the two swing normal legs and the integrated limb serving as an arm change. The footholds of these three limbs that consist of a regular triangle evolve to the hexapod gait. It is a reverse process between the switch from the hexapod gait to pentapod gait and the switch from the pentapod gait to the hexapod gait.

Figure 16 shows the stability of the robot between

hexapod gait and pentapod gait. The regular hexagon circumscribed of the hexapod gait is the same as the regular pentagon circumscribed of the pentapod gait, and its radius is CR . The maximum stability $Ch2$ of the robot with six-limb support is $\frac{\sqrt{3}}{2}CR$, and the maximum stability $Ch1$ of the robot with three-limb support is $0.5CR$. The maximum stability point of the robot with six-limb symmetrical support or three-limb symmetrical support is the geometric center. The maximum stability $Cp2$ of the robot with five-limb support is approximately $0.809CR$, and the maximum stability $Cp1$ of the robot with three-limb support is approximately $0.427CR$. The maximum stability point of the robot with five-limb symmetrical support is the gravity center. However, the geometric center stability of the robot with three-limb symmetrical support is $0.309CR$ and lower than the maximum stability. The distance between the geometric center and the maximum stability point is $0.118CR$. The whole hexapod gait stability is better than the whole pentapod gait stability.

4.2 Pentapod gait

The integrated limb serves as a five-DOF arm while the robot walks with pentapod gait. According to the states of all limbs for the hexapod robot, the pentapod gait can be divided into three types: 4+1 gait, 3+2 gait, and mixture pentapod gait.

The slowest gait among these three typical pentapod gaits is the 4+1 gait. In a 4+1 gait cycle, the robot

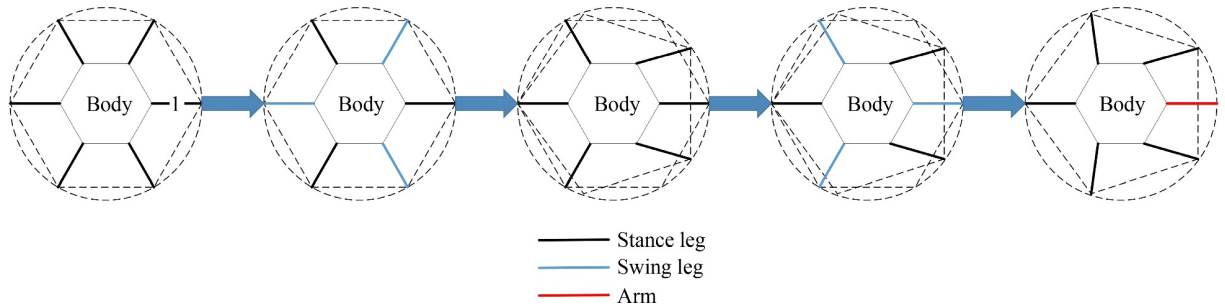


Fig. 14 Switch from hexapod gait to pentapod gait of hexapod robot.

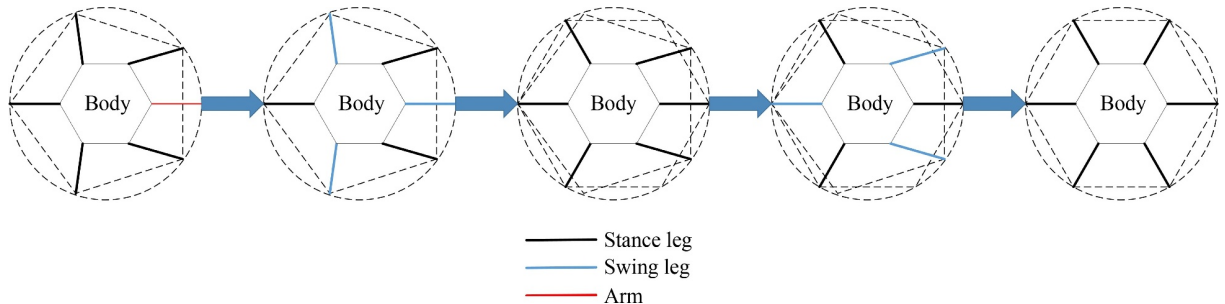


Fig. 15 Switch from pentapod gait to hexapod gait of hexapod robot.

possesses four stance limbs and one swing limb. A periodic 4+1 gait can be decomposed into five steps, as shown in Fig. 17.

The fastest gait among these three typical pentapod gaits is the 3+2 gait, as shown in Fig. 18. In a 3+2 gait cycle, the robot possesses three stance limbs and two swing limbs. Owing to the odd number of limbs, every

limb needs to move two times in a gait cycle for the 3+2 pentapod gait. The support polygon stays the same triangle in the whole 3+2 pentapod gait with the symmetrical limbs.

The velocity of the mixture pentapod gait is between the 4+1 pentapod gait and the 3+2 pentapod gait. The mixture pentapod gait can be divided into three steps, as shown in Fig. 19. In the first and second steps, the robot possesses three stance limbs and two swing limbs. In the last step, the robot possesses four stance limbs and one swing limb.

The maximum stability of the pentapod gait with four support limbs is more than the pentapod gait with three support limbs, but the stability of the robot geometrical center with four support limbs is the same as the robot with three support limbs. For all pentapod gaits, the stability of the geometrical center is approximately $0.309CR$. Considering the hexapod robot with integrated limbs in the real world, the real gravity center is located

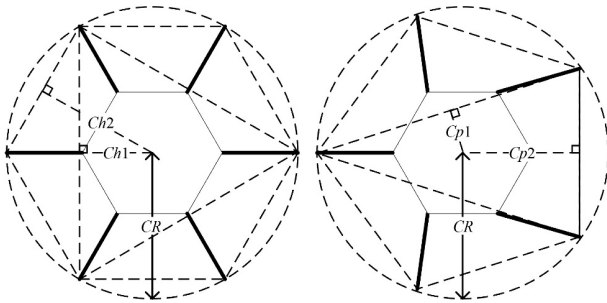


Fig. 16 Stability of hexapod gait and pentapod gait.

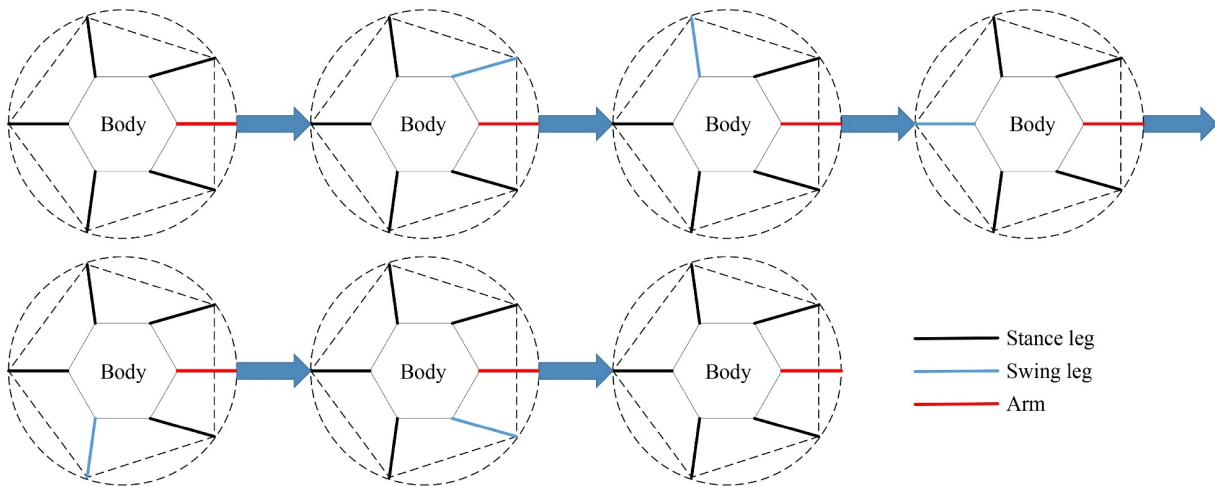


Fig. 17 4+1 pentapod gait of hexapod robot.

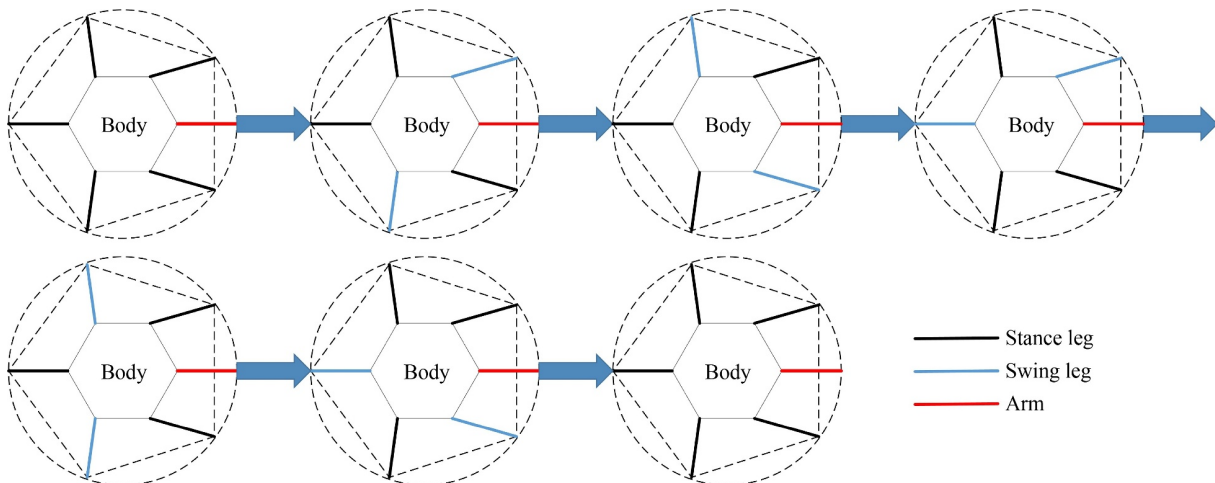


Fig. 18 3+2 pentapod gait of hexapod robot.

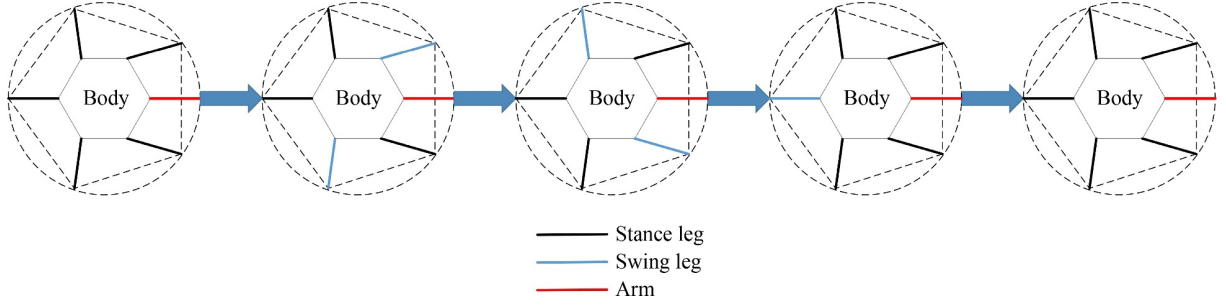


Fig. 19 Mixed pentapod gait of hexapod robot.

in the integrated limb direction, and changing the object position manipulated by the integrated limb can increase the stability while the robot walks with pentapod gait.

4.3 Manipulation of integrated limb

The normal leg of the radial symmetrical hexapod robot is typical and not discussed. In this section, the integrated limb of this novel hexapod robot is discussed in detail. The screw motion and the angle of the j th joint in the i th limb are denoted as ξ_{ij} and θ_{ij} , respectively.

The forward kinematics of the integrated limb in $\{O_g\}$ is given by the product of exponentials:

$${}^{O_g} \mathbf{g} = {}^{O_g}{}_{COB} \mathbf{g} {}^{COB}{}_{O_i} \mathbf{g} e^{\theta_{11}\xi_{11}} e^{\theta_{21}\xi_{12}} e^{\theta_{31}\xi_{13}} e^{\theta_{41}\xi_{14}} e^{\theta_{51}\xi_{15}} {}^{O_i} \mathbf{g}(0), \quad (19)$$

$$\begin{aligned} {}^{O_1} \mathbf{g} &= e^{\theta_{11}\xi_{11}} e^{\theta_{21}\xi_{12}} e^{\theta_{31}\xi_{13}} e^{\theta_{41}\xi_{14}} e^{\theta_{51}\xi_{15}} {}^{O_1} \mathbf{g}(0) = \begin{bmatrix} {}^{O_1} \mathbf{R} & \mathbf{P}_{E_1}^{O_1} \\ \mathbf{0} & 1 \end{bmatrix} = \begin{bmatrix} r_{11} & r_{12} & r_{13} & x_{E_1}^{O_1} \\ r_{21} & r_{22} & r_{23} & y_{E_1}^{O_1} \\ r_{31} & r_{32} & r_{33} & z_{E_1}^{O_1} \\ 0 & 0 & 0 & 1 \end{bmatrix} \\ &= \begin{bmatrix} c\theta_{11}c\theta_{1x}c\theta_{15} - s\theta_{11}s\theta_{15} & -c\theta_{11}c\theta_{1x}s\theta_{15} - s\theta_{11}c\theta_{15} & c\theta_{11}s\theta_{1x} & a_{E_1}^{O_1}c\theta_{11} + l_5r_{11} \\ c\theta_{11}c\theta_{1x}c\theta_{15} + c\theta_{11}s\theta_{15} & -s\theta_{11}c\theta_{1x}s\theta_{15} + c\theta_{11}c\theta_{15} & s\theta_{11}s\theta_{1x} & a_{E_1}^{O_1}s\theta_{11} + l_5r_{21} \\ -s\theta_{1x}c\theta_{15} & s\theta_{1x}s\theta_{15} & c\theta_{1x} & b_{E_1}^{O_1} + l_5r_{31} \\ 0 & 0 & 0 & 1 \end{bmatrix}, \end{aligned} \quad (20)$$

where $s = \sin$, $c = \cos$, and

$$\theta_{1x} = \theta_{12} + \theta_{13} + \theta_{14},$$

$$a_{E_1}^{O_1} = l_1 + l_2c\theta_{12} + l_{31}c(\theta_{12} + \theta_{13}) + l_4c(\theta_{12} + \theta_{13} + \theta_{14}),$$

$$b_{E_1}^{O_1} = l_2s\theta_{12} + l_{31}s(\theta_{12} + \theta_{13}) + l_4s(\theta_{12} + \theta_{13} + \theta_{14}),$$

$${}^{O_1} \mathbf{g}(0) = \begin{bmatrix} 1 & 0 & 0 & l_1 + l_2 + l_{31} + l_4 + l_5 \\ 0 & 1 & 0 & 0 \\ 0 & 0 & 1 & 0 \\ 0 & 0 & 0 & 1 \end{bmatrix}.$$

The attitude of the expected pose is difficult to be compensated for the lacked dimension. The horizontal position that is perpendicular to the move direction of the robot body is compensated for the integrated limb while the robot walks.

${}^{O_1} \mathbf{g}$ can also be expressed as follows:

where ${}^{O_g} \mathbf{g} \in SE(3)$ represents the expected pose of the i th limb end-effector in $\{O_g\}$, ${}^{O_g}{}_{COB} \mathbf{g} \in SE(3)$ represents the position and the attitude of the robot body in $\{O_g\}$, ${}^{COB}{}_{O_i} \mathbf{g} \in SE(3)$ represents the pose of i th limb coordinate in $\{COB\}$, and ${}^{O_i} \mathbf{g}(0) \in SE(3)$ is the initial pose of the i th limb end-effector in the i th limb coordinate. In this section, integrated Limb 1 is selected as the analysis object.

The integrated limb DOF of the hexapod robot lacks one dimension for the whole the expected pose space. Hence, the one dimension lacked can be compensated by utilizing the redundant DOF of the robot body. Integrated Limb 1 serves as the arm while the robot walks with pentapod gait. The forward kinematics of the integrated limb in $\{O_1\}$ can be simplified into the following:

$$\begin{aligned} {}^{O_1} \mathbf{g} &= \begin{bmatrix} {}^{O_1} \mathbf{R} & \mathbf{P}_{E_1}^{O_1} \\ \mathbf{0} & 1 \end{bmatrix} \\ &= \begin{bmatrix} ({}^{O_g} \mathbf{R})^T {}^{O_g}{}_{E_1} \mathbf{R} & ({}^{O_g} \mathbf{R})^T (\mathbf{P}_{E_1}^{O_g} - \mathbf{P}_{COB}^{O_g}) - \mathbf{P}_{O_1}^{COB} \\ \mathbf{0} & 1 \end{bmatrix}, \end{aligned} \quad (21)$$

where ${}^{O_g} \mathbf{g} = \begin{bmatrix} {}^{O_g} \mathbf{R} & \mathbf{P}_{COB}^{O_g} \\ \mathbf{0} & 1 \end{bmatrix}$, ${}^{O_g}{}_{E_1} \mathbf{g} = \begin{bmatrix} {}^{O_g} \mathbf{R} & \mathbf{P}_{E_1}^{O_g} \\ \mathbf{0} & 1 \end{bmatrix}$, $\mathbf{P}_{O_1}^{COB}$ represents the position $[R_B \ 0 \ 0]^T$ of the robot body in $\{COB\}$, and R_B represents the length from the geometrical center of the body to the origin of $\{O_1\}$.

To simplify the inverse kinematics of mobile manipulation, the workspace of θ_{12} , θ_{13} , and θ_{14} can be equivalent to the planar motion of θ_{1x} , $a_{E_1}^{O_1}$, and $b_{E_1}^{O_1}$ with a boundary condition. The boundary condition with the solution can be expressed as follows:

$$(a_{E_1}^{O_1} - l_1)^2 + (b_{E_1}^{O_1})^2 \leq (l_2 + l_{31} + l_4)^2. \quad (22)$$

Therefore, the solution of θ_{11} , θ_{15} , θ_{1x} , $a_{E_1}^{O_1}$, and $b_{E_1}^{O_1}$ is

equivalent to the inverse kinematics of the integrated limb in all cases.

The position compensation of the robot body in $\{O_g\}$ can be expressed as $d\mathbf{P}_{COB}^{O_s} = dl \begin{bmatrix} \sin\theta_b^{O_s} & -\cos\theta_b^{O_s} & 0 \end{bmatrix}^T$. dl is the unknown position compensation, and $\theta_b^{O_s}$ is the known angle between the robot movement direction and the x -axis in $\{O_g\}$.

$\mathbf{P}_{E_1}^{O_1}$ can be expressed as follows:

$$\mathbf{P}_{E_1}^{O_1} = \begin{bmatrix} x_{E_1}^{O_1} \\ y_{E_1}^{O_1} \\ z_{E_1}^{O_1} \end{bmatrix} + dl \begin{bmatrix} \sin\theta_b^{COB} \\ -\cos\theta_b^{COB} \\ 0 \end{bmatrix}, \quad (23)$$

where $\begin{bmatrix} x_{E_1}^{O_1} & y_{E_1}^{O_1} & z_{E_1}^{O_1} \end{bmatrix}^T = (\mathbf{P}_{COB}^{O_s} \mathbf{R})^T (\mathbf{P}_{E_1}^{O_s} - \mathbf{P}_{COB,0}^{O_s}) - \mathbf{P}_{O_1}^{COB}$, $\mathbf{P}_{COB,0}^{O_s}$ represents the initial position of the robot body without compensation in $\{O_g\}$, and $\mathbf{P}_{COB}^{O_s} = \mathbf{P}_{COB,0}^{O_s} + d\mathbf{P}_{COB}^{O_s}$ is the real position of the robot body.

Moreover,

$$\begin{bmatrix} \sin\theta_b^{COB} & -\cos\theta_b^{COB} & 0 \end{bmatrix} = \begin{bmatrix} O_s \\ COB \end{bmatrix} \mathbf{R}^T \begin{bmatrix} \sin\theta_b^{O_s} & -\cos\theta_b^{O_s} & 0 \end{bmatrix}^T. \quad (24)$$

Equation (24) is the known unit compensation in the $\{COB\}$ coordinate while the robot body is always parallel to the supporting plane formed with supporting feet.

Then, the inverse kinematics of the integrated limb can be divided into two cases:

1) If $|\cos\theta_{1x}| \geq 1$, a solution exists for the integrated limb with the compensation of the robot body to increase the workspace.

2) If $|\cos\theta_{1x}| < 1$, the position error of the integrated limb can be compensated by the position of the robot body.

Case 1:

In the first case, the local inverse kinematics of the integrated limb using Eq. (22) can be written as follows:

$$\begin{cases} \theta_{1x} = \arccos r_{33}, \\ b_{E_1}^{O_1} = z_{E_1}^{O_1}. \end{cases} \quad (25)$$

The inverse solution (Case 1.4) without the compensation while satisfying the boundary condition Eq. (22) can be written as follows:

$$\begin{cases} a_{E_1}^{O_1} = \sqrt{(x_{E_1}^{O_1} - l_5 r_{11})^2 + (y_{E_1}^{O_1} - l_5 r_{21})^2}, \\ \theta_{11} = \arctan 2(y_{E_1}^{O_1} - l_5 r_{21}, x_{E_1}^{O_1} - l_5 r_{11}), \\ \theta_{15} = \frac{\arctan 2(r_{11}, r_{21}) - \theta_{11}}{r_{33}}, \\ dl = 0. \end{cases} \quad (26)$$

The inverse solution (Case 1.3) with the compensation while satisfying the boundary condition Eq. (22) can be written as follows:

$$\begin{cases} dl = \frac{-B + \sqrt{B^2 - 4C}}{2}, \\ a_{E_1}^{O_1} = \sqrt{(x_{E_1}^{O_1} - l_5 r_{11} - dl \sin\theta_b^{COB})^2 + (y_{E_1}^{O_1} - l_5 r_{21} + dl \cos\theta_b^{COB})^2}, \\ \theta_{11} = \arctan 2(y_{E_1}^{O_1} - l_5 r_{21} + dl \cos\theta_b^{COB}, x_{E_1}^{O_1} - l_5 r_{11} - dl \sin\theta_b^{COB}), \\ \theta_{15} = \frac{\arctan 2(r_{11}, r_{21}) - \theta_{11}}{r_{33}}, \end{cases} \quad (27)$$

where $B = -2[(x_{E_1}^{O_1} - l_5 r_{11}) \sin\theta_b^{COB} - (y_{E_1}^{O_1} - l_5 r_{21}) \cos\theta_b^{COB}]$, and $C = (x_{E_1}^{O_1} - l_5 r_{11})^2 + (y_{E_1}^{O_1} - l_5 r_{21})^2 - \left[\sqrt{(l_2 + l_{31} + l_4)^2 - (b_{E_1}^{O_1})^2} + l_1 \right]^2$.

When $B^2 - 4C < 0$, no solution (Case 1.1) exists with the compensation, and the point is not in the workspace of the integrated limb. When dl cannot satisfy the stability of the robot, no solution exists (Case 1.2).

Case 2:

In the second case, θ_{11} , θ_{1x} , and θ_{15} can be solved by the attitude of the end-effector expected pose, and the local inverse kinematics of ${}_{E_1}^{O_1} \mathbf{R} = (\mathbf{P}_{COB}^{O_s} \mathbf{R})^T {}_{E_1}^{O_s} \mathbf{R}$ can be written as follows:

$$\begin{cases} \theta_{11} = \arctan 2(r_{13}, r_{23}), \\ \theta_{15} = \arctan 2(-r_{31}, r_{32}), \\ \theta_{1x} = \arctan 2(r_{33}, r_{13} \cos\theta_{11} + r_{23} \sin\theta_{11}). \end{cases} \quad (28)$$

When the direction of the robot movement is perpendicular to the orientation of θ_{11} , many solutions exist (Case 2.4), in which minimum compensation with the boundary condition Eq. (22) is selected if θ_{11} is equal to $\arctan 2(y_{E_1}^{O_1} - l_5 r_{21}, x_{E_1}^{O_1} - l_5 r_{11})$, and no solution exists (Case 2.1) if θ_{11} is unequal to $\arctan 2(y_{E_1}^{O_1} - l_5 r_{21}, x_{E_1}^{O_1} - l_5 r_{11})$.

When the direction of the robot movement is not perpendicular to the orientation of θ_{11} , the inverse position (Case 2.3) of the integrated limb with the body compensation can be expressed as follows:

$$\begin{cases} b_{E_1}^{O_1} = z_{E_1}^{O_1} - l_5 r_{31}, \\ a_{E_1}^{O_1} = \frac{(y_{E_1}^{O_1} - r_{21} l_5) \sin\theta_b^{COB} - (r_{11} l_5 - x_{E_1}^{O_1}) \cos\theta_b^{COB}}{\cos(\theta_{11} - \theta_b^{COB})}, \\ dl = \frac{x_{E_1}^{O_1} \sin\theta_{11} - y_{E_1}^{O_1} \cos\theta_{11} + (r_{21} \cos\theta_{11} - r_{11} \sin\theta_{11}) l_5}{\cos(\theta_{11} - \theta_b^{COB})}. \end{cases} \quad (29)$$

If the direction of the robot movement is the same as the orientation of θ_{11} , the minimum compensation is as follows:

$$dl = x_{E_1}^{O_1} \sin\theta_{11} - y_{E_1}^{O_1} \cos\theta_{11} + (r_{21} \cos\theta_{11} - r_{11} \sin\theta_{11}) l_5. \quad (30)$$

When dl cannot satisfy the stability of the robot, no solution exists (Case 2.2).

In all cases of the inverse kinematics, the inverse kinematics of θ_{12} , θ_{13} , and θ_{14} can be written as follows while the equivalent solution satisfies Eq. (22):

$$\begin{cases} t_a = a_{E_1}^{O_1} - l_1 - l_4 \cos \theta_{1x}, \\ t_b = b_{E_1}^{O_1} - l_4 \sin \theta_{1x}, \\ s = \sqrt{t_a^2 + t_b^2}, \\ \theta_{12} = \arctan 2(t_a, t_b) \pm \arccos \frac{s^2 + l_2^2 - l_{31}^2}{2sl_2}, \\ \theta_{13} = \pm \arccos \frac{l_2^2 + l_{31}^2 - s^2}{2l_2l_{31}} - \pi, \\ \theta_{14} = \theta_{1x} - \theta_{12} - \theta_{13}. \end{cases} \quad (31)$$

One of two solutions for the first case is selected according to the geometry of the integrated limb.

The compensation of the robot body is limited because of the pentapod gait stability. In the omnidirectional pentapod gait, the omnidirectional compensation utilizing the robot body position is considered for minimum stability, and maximum omnidirectional compensation is approximately $0.118CR$.

The mobile manipulation compensation of the hexapod robot in horizontal plane can be expressed as Fig. 20.

5 Experiments

Two kinds of manipulation conditions including several manipulation cases are introduced in the previous sections. The manipulation performance of the robot is verified through corresponding experiments in this section.

5.1 Experiment of fixed coordinated clamping with two adjacent integrated limbs

The experiment of clamping with two adjacent integrated limbs is implemented. In this experiment, the robot should clamp a relatively large object by using two adjacent integrated limbs. According to this requirement, corresponding movements of the robot are planned and

executed as shown in Fig. 21. Figure 21(a) shows the initial standing pose of the robot. The switch to manipulation status is shown in Figs. 21(b) and 21(c). During this process, the four remaining supporting legs adjust the body pose to maintain the stability of the robot. The robot realizes the coordinated clamping task in Figs. 21(d) and 21(e). Figures 21(f)–21(i) show the switch from manipulation status to supporting status. In this experiment, two integrated leg–arm limbs complete the coordinated clamping task while the four remaining legs adjust the robot pose to change the position of the gravity center of the robot and the object to maintain stability.

5.2 Experiment of fixed coordinated shearing with two adjacent integrated limbs

One of the integrated limbs has a gripper, and the other has a scissors. Hence, coordinated shearing manipulation can be achieved by using these two integrated limbs. The gripper can grab the object, and the scissors can clip it. An experiment in terms of solving the coordinated shearing task with this robot is carried out. Based on the task strategy shown in Fig. 13, the experiment process is shown in Fig. 22. The initial standing pose shown in Figs. 22(a)–22(c) demonstrates the switch of integrated limbs from supporting status to manipulation status. The main limb with the gripper approaches the object and clamps the rigid rope in Fig. 22(d). Figures 22(e) and 22(f) represent shearing, where the end-effectors of the two limbs move to the coordinated working space and shear the object. Figures 22(g)–22(i) show the switch from manipulation status to supporting status, and can be regarded as the inverse process of the first stage. The coordinated manipulation feasibility of shearing and switching flexibility between different working modes of the novel integrated limb structure are verified through this experiment.

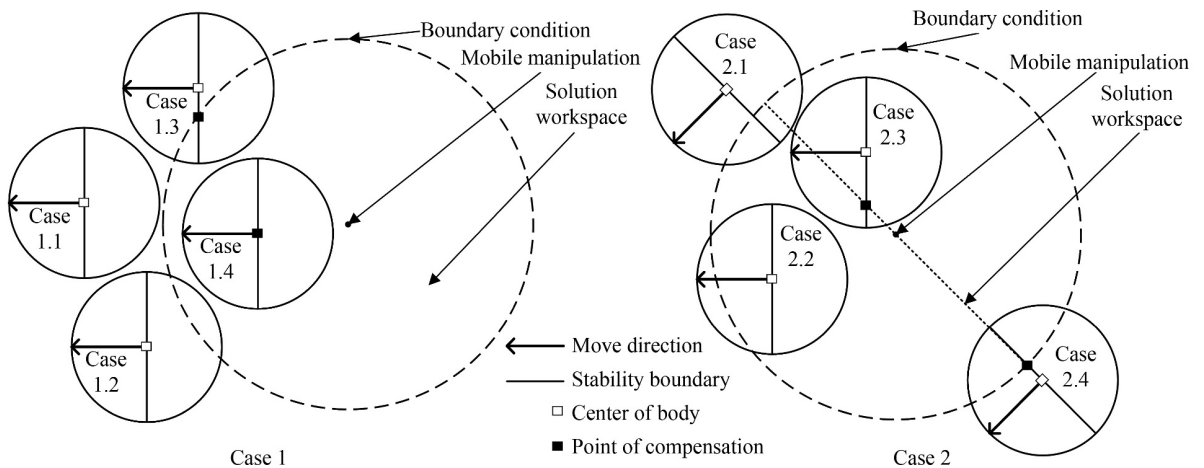


Fig. 20 Mobile manipulation solution of hexapod robot.

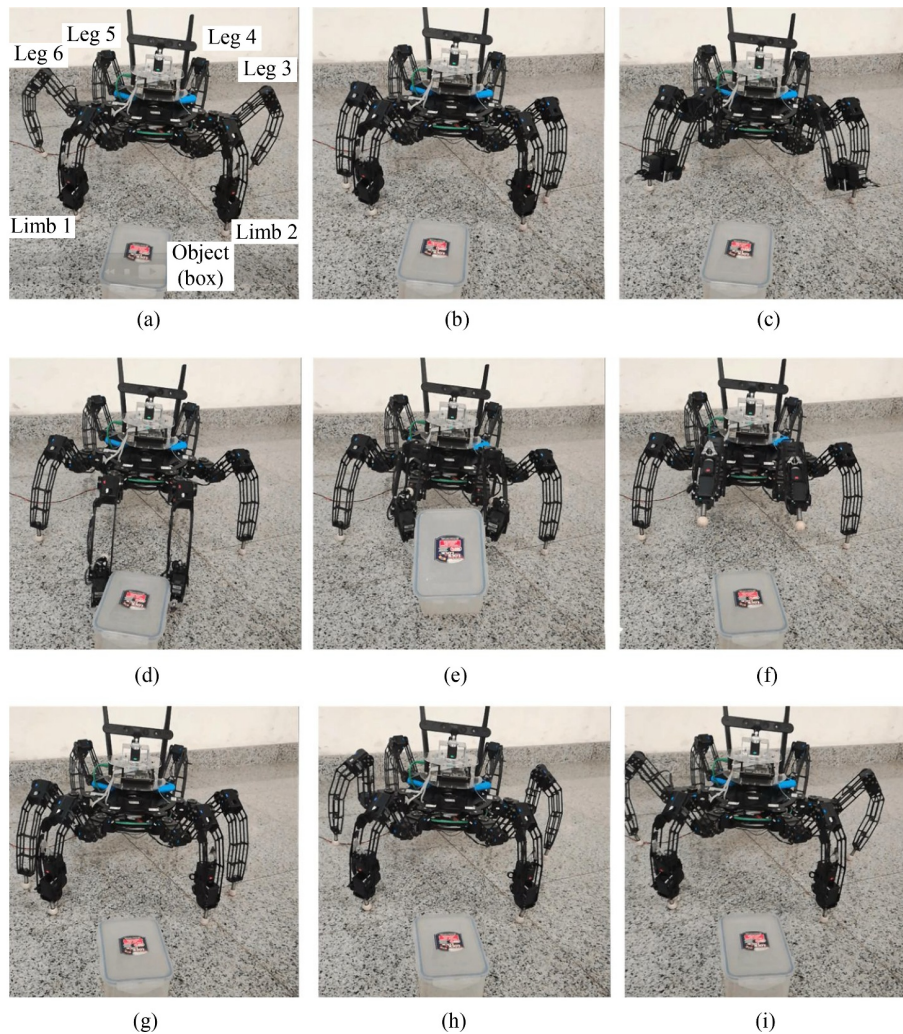


Fig. 21 Coordinated clamping by using two adjacent integrated limbs: (a) initial condition of robot; (b) Legs 3 and 4 swing forward, and the four normal legs switch to stable supporting status; (c) two integrated limbs (Limbs 1 and 2) are lifted and switch to manipulation status; (d) the robot clamps the object (box) by using two integrated limbs; (e) the robot lifts the object; (f) the robot puts down the object, and two integrated limbs switch to walking status; (g) two integrated limbs return to supporting status; (h) two bilateral intermediate legs (Legs 3 and 6) are lifted; (i) Legs 3 and 6 swing backward and are put down, and the robot switches to the status of six-limb support.

5.3 Experiment of mobile manipulation with one integrated limb

As the mobile manipulation function presented in Section 4, the initial condition of the robot is hexapod gait ending and six-limb support, then the robot changes to pentapod gait while one integrated leg–arm limb (Limb 1 that is equipped with gripper) switches to manipulation status. In this case, Limb 2 works as the normal leg. The mobile manipulation mode of this robot utilizes the mixture pentapod gait because the velocity of mixture pentapod gait is faster than that of 4+1 pentapod gait, and the maximum stability is higher than that of 3+2 pentapod gait. Based on these conditions, a mobile manipulation experiment is carried out to verify the effectiveness and the flexibility of the integrated leg–arm limb mechanism. Figure 23(a) shows that the robot ends hexapod gait

walking and is in six-limb supporting status. Figures 23(b)–23(e) show the switch of robot from hexapod gait to pentapod gait. Moreover, in this process, the integrated leg–arm limb with gripper (Limb 1) is transformed into manipulation status and clamps the object, as shown in Fig. 23(e). Figures 23(f)–23(i) represent the process of robot walking with mixture pentapod gait while clamping the object. During mobile manipulation, the robot body keeps moving to compensate the position deviation.

6 Conclusions

A novel integrated leg–arm hexapod robot with an omnidirectional body is developed in this paper. The mechanical structure of the integrated leg–arm limb is designed to realize functions of the leg and the arm.

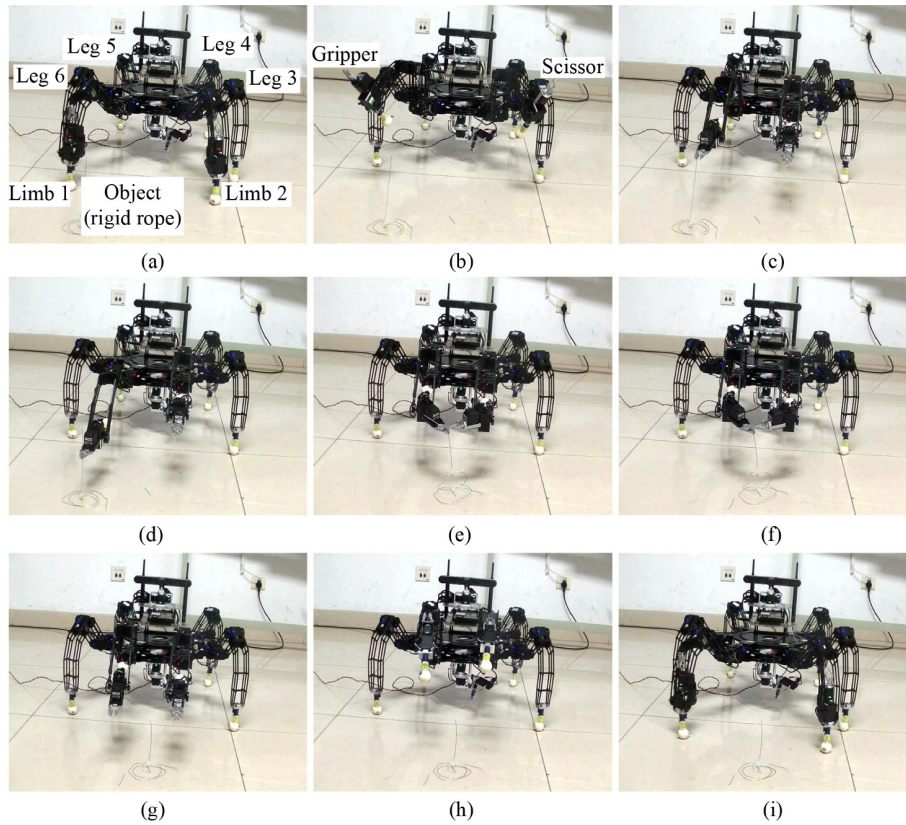


Fig. 22 Coordinated shearing by using two adjacent integrated limbs: (a) initial condition of the robot; (b) four normal legs switch to stable supporting status, and two integrated limbs (Limbs 1 and 2) are lifted and start switching to manipulation status; (c) two integrated limbs switch to manipulation status; (d) the main limb (Limb 1) with the gripper approaches the object and clamps the rigid rope; (e) the end-effectors of two limbs move to the coordinated working space; (f) the slave limb (Limb 2) with the scissors shears off the rigid rope; (g) the main limb puts down the object and prepares for switching to walking status with the slave limb; (h) two integrated limbs switch to walking status; (i) the robot returns to the status of six-limb support.

Based on this structure, the switching method between the leg and the arm is presented. Therefore, the robot can walk with all limbs and manipulate with two integrated leg–arm limbs. Compared with the normal multilegged robot that can perform the manipulation task, this novel leg–arm mechanism integrates the walking leg and the manipulator as a system. No redundant DOF is required, and cost and working space can be saved. As a result, interference is reduced, and the manipulation task can be performed in a more flexible, smoother manner.

For the analysis of this robot in manipulation mode, first, the main manipulation mode is divided into two types according to the number of integrated limbs involved in the task. When two integrated limbs are applied to solve the working task, this manipulation condition mainly includes fixed coordinated clamping case and fixed coordinated shearing case. While the robot lifts its one single integrated limb, it can accomplish mobile manipulation with pentapod gait.

Different fixed coordinated manipulation analyses are conducted. The stable clamping force constraint condition, the DOF analysis of equivalent PM by using screw theory, and the constraint equation of two integrated limbs are determined in the fixed coordinated clamping

case. In the fixed coordinated shearing case, the concept of ideal coordinated manipulation ball is presented based on the coordinated working space to guide the coordinated shearing task, and the constraint analysis of two adjacent integrated limbs is performed. Moreover, the fixed coordinated shearing task strategy is introduced to accomplish the task. Then, the concept of mobile manipulation is presented: A complex six-DOF manipulation can be achieved with compensation while the stability and the walk velocity of the robot are reduced. In this condition, the gait switching analysis between hexapod gait and pentapod gait, and different pentapod gaits analysis are discussed as well.

Corresponding experiments of different manipulation conditions of the robot are implemented. The results demonstrate a good manipulation performance of the robot with its integrated leg–arm limbs. This novel integrated leg–arm robot can be equipped with more end-effectors on the tip of its integrated limbs to realize more manipulation functions. It can be applied in many different fields because of its good performance including locomotion function, fixed manipulation function, and mobile manipulation function, such as city security, antiterrorism manipulation, and planetary exploration.

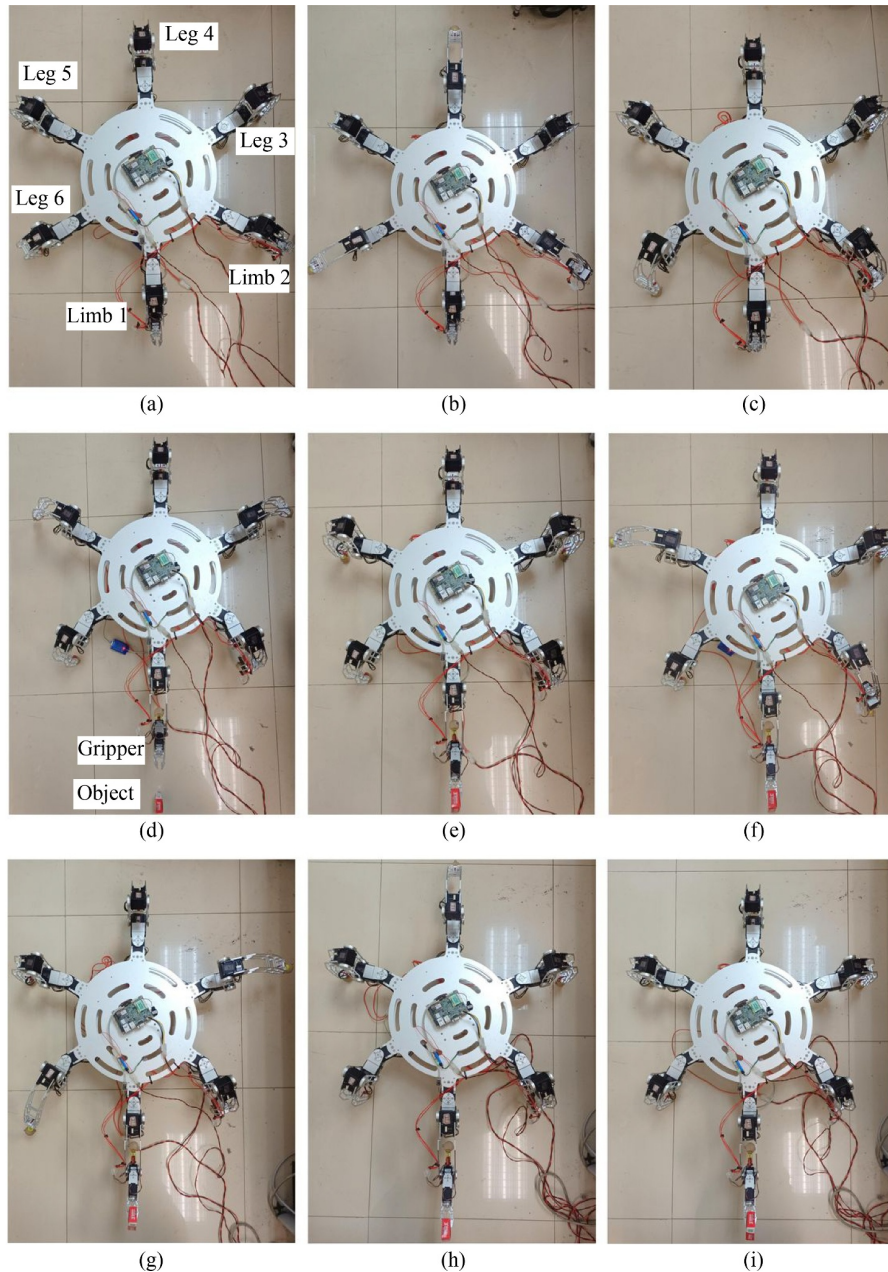


Fig. 23 Robot mobile manipulation: (a) Initial condition of robot is six-limb supporting status; (b) three limbs that include one integrated limb (Limb 2) and two normal legs (Legs 4 and 6) are lifted; (c) the lifted limbs swing to the planned pose and switch to supporting status; (d) Limb 1 and Legs 3 and 5 are lifted while Limb 1 that is equipped with gripper starts switching to manipulation status; (e) two lifted normal legs (Legs 3 and 5) swing to the planned pose and switch to supporting status while Limb 1 clamps the object; (f) Limb 2 and Leg 5 are lifted and swing to the planned pose; (g) the lifted limbs switch to supporting status while Legs 3 and 6 are lifted and swing to the planned pose; (h) the lifted limbs switch to supporting status while Leg 4 is lifted; (i) Leg 4 swings to the planned pose and switches to supporting status, and then the robot is in the status of five-limb support that is considered as the initial condition of the next mixture pentapod gait cycle.

Nomenclature

Variables

$Ch1$	Maximum stability of robot with three-limb support in hexapod gait	$Ch2$	Maximum stability of robot with six-limb support in hexapod gait
		$Cp1$	Maximum stability of robot with three-limb support in pentapod gait
		$Cp2$	Maximum stability of robot with five-limb support in pentapod gait

CR	Radius of the regular hexagon circumscribed in hexapod gait and pentapod gait
d	Order of the mechanism
f_{iz}	Component force along the z -axis ($\{C_i\}$) that is effected on the object of each limb end
df	DOF of equivalent PM
F_g	Gravity of object
${}^{O_i}g$	Expected pose of i th limb end-effector in $\{O_g\}$
${}^{COB}g$	Position and attitude of robot body in $\{O_g\}$
${}^{COB}g$	Pose of the i th limb coordinate in $\{COB\}$
${}^{O_i}g(0)$	Initial pose of the i th limb end-effector in the i th limb coordinate
k	Number of kinematic pairs
$l_{3k} (k = 1, 2)$	Lengths of Shanks 1 and 2
l_i, l_s, l_j, l_K	Lengths of E_1L , SK , JK , and KE_2 in Fig. 11
$l_m (m = 1, 2, \dots, 5)$	Lengths of hip, thigh, shank, Arm 1, and Arm 2
dl	Unknown position compensation
n	Total number of links
P	Position vector
$dP_{COB}^{O_g}$	Position compensation of robot body in $\{O_g\}$
$P_{COB,0}^{O_g}$	Initial position of robot body without compensation in $\{O_g\}$
$P_{COB}^{O_g}$	Real position of robot body
R_B	Radius of robot body
R_i	Diameter of ideal coordinated manipulation ball
R	Rotation matrix
$S_{br}i$	Twist system of branch i
S_{br}^r	Constrained wrench system of branch i
S_m	Twist system of equivalent PM
S^c	Constrained wrench system of equivalent PM
S^r	Constrained wrench system of moving platform
α	Angle between E_1E_2 and E_1L in Fig. 11
ε	Number of virtual constraints
ζ	Passive DOF
ρ	Number of branches
λ	Number of independent common constraints
$\mu (\mu \in [1, 4])$	Static friction coefficient between limb end and object
$\theta_b^{O_g}$	Known angle between robot movement direction and x -axis in $\{O_g\}$
θ_{ij} ($i = 3, 4, 5, 6; j = 1, 2, 3$)	Rotation angle of every joint in normal leg
θ_{ij} ($i = 1, 2; j = 1, 2, \dots, 5$) _{limb}	Rotation angle of every joint in integrated leg–arm
φ_i	DOF of the i th kinematic pair
\mathcal{S}_j	Twist of the j th joint in the i th limb
ξ_{ij}	Screw motion of the j th joint in the i th limb

Acknowledgements This paper was funded by the National Key R&D

Program of China (Grant No. 2019YFB1309600) and the National Natural Science Foundation of China (Grant Nos. 51775011 and 91748201).

Open Access This article is licensed under a Creative Commons Attribution 4.0 International License, which permits use, sharing, adaptation, distribution, and reproduction in any medium or format as long as appropriate credit is given to the original author(s) and source, a link to the Creative Commons license is provided, and the changes made are indicated.

The images or other third-party material in this article are included in the article's Creative Commons license, unless indicated otherwise in a credit line to the material. If material is not included in the article's Creative Commons license and your intended use is not permitted by statutory regulation or exceeds the permitted use, you will need to obtain permission directly from the copyright holder.

Visit <http://creativecommons.org/licenses/by/4.0/> to view a copy of this license.

References

- Gullan P J, Cranston P S. The Insects: An Outline of Entomology. 5th ed. Hoboken: John Wiley & Sons, 2014
- Koyachi N, Arai T, Adachi H, Itoh Y. Integrated limb mechanism of manipulation and locomotion for dismantling robot-basic concept for control and mechanism. In: Proceedings of 1993 IEEE/Tsukuba International Workshop on Advanced Robotics. Tsukuba: IEEE, 1993, 81–84
- Takahashi Y, Arai T, Mae Y, Inoue K, Koyachi N. Development of multi-limb robot with omnidirectional manipulability and mobility. In: Proceedings of 2000 IEEE/RSJ International Conference on Intelligent Robots and Systems (IROS 2000) (Cat. No. 00CH37113). Takamatsu: IEEE, 2000, 3: 2012–2017
- Mae Y, Arai T, Inoue K, Miyawaki K. Application of a ‘limb mechanism’ robot to rescue tasks. Advanced Robotics, 2002, 16(6): 529–532
- Hirose S, Yoneda K, Arai K, Ibe T. Design of a quadruped walking vehicle for dynamic walking and stair climbing. Advanced Robotics, 1994, 9(2): 107–124
- Hirose S, Yoneda K, Arai K, Ibe T. Design of prismatic quadruped walking vehicle TITAN VI. Journal of the Robotics Society of Japan, 1991, 9(4): 445–452
- Hirose S, Yoneda K, Tsukagoshi H. TITAN VII: quadruped walking and manipulating robot on a steep slope. In: Proceedings of International Conference on Robotics and Automation. Albuquerque: IEEE, 1997, 1: 494–500
- Arikawa K, Hirose S. Development of quadruped walking robot TITAN-VIII. In: Proceedings of IEEE/RSJ International Conference on Intelligent Robots and Systems. IROS '96. Osaka: IEEE, 1996, 1: 208–214
- Hirose S, Kato K. Development of quadruped walking robot with the mission of mine detection and removal-proposal of shape-feedback master-slave arm. In: Proceedings of 1998 IEEE International Conference on Robotics and Automation (Cat. No. 98CH36146). Leuven: IEEE, 1998, 2: 1713–1718
- Kato K, Hirose S. Development of the quadruped walking robot, “TITAN-IX”. In: Proceedings of 2000 the 26th Annual Conference

- of the IEEE Industrial Electronics Society. IECON 2000. 2000 IEEE International Conference on Industrial Electronics, Control and Instrumentation. 21st Century Technologies. Nagoya: IEEE, 2000, 1: 40–45
11. Takubo T, Arai T, Inoue K, Ochi H, Konishi T, Tsurutani T, Hayashibara Y, Koyanagi E. Integrated limb mechanism robot ASTERISK. *Journal of Robotics and Mechatronics*, 2006, 18(2): 203–214
 12. Chen X B, Gao F, Qi C K, Tian X H, Zhang J Q. Spring parameters design for the new hydraulic actuated quadruped robot. *Journal of Mechanisms and Robotics*, 2014, 6(2): 021003
 13. Bai S P, Low K H. Terrain evaluation and its application to path planning for walking machines. *Advanced Robotics*, 2001, 15(7): 729–748
 14. Bai S P, Low K H, Teo M Y. Path generation of walking machines in 3D terrain. In: *Proceedings of 2002 IEEE International Conference on Robotics and Automation (Cat. No. 02CH37292)*. Washington, DC: IEEE, 2002, 3: 2216–2221
 15. Bellicoso C D, Krämer K, Stäuble M, Sako D, Jenelten F, Bjelonic M, Hutter M. Alma-articulated locomotion and manipulation for a torque-controllable robot. In: *Proceedings of 2019 International Conference on Robotics and Automation (ICRA)*. Montreal: IEEE, 2019, 8477–8483
 16. Bhavanibhatla K, Suresh-Fazeela S, Pratihari D K. A study on determining optimal base location of a serial manipulator mounted on a hexapod mobile robot. *Journal of the Brazilian Society of Mechanical Sciences and Engineering*, 2021, 43(4): 226
 17. Liu J M, Tian Y, Gao F. A novel six-legged walking machine tool for *in-situ* operations. *Frontiers of Mechanical Engineering*, 2020, 15(3): 351–364
 18. He J, Gao F. Mechanism, actuation, perception, and control of highly dynamic multilegged robots: a review. *Chinese Journal of Mechanical Engineering*, 2020, 33(1): 79
 19. Niquille S C. Regarding the pain of SpotMini: Or what a robot's struggle to learn reveals about the built environment. *Architectural Design*, 2019, 89(1): 84–91
 20. Ding X L, Yang F. Study on hexapod robot manipulation using legs. *Robotica*, 2016, 34(2): 468–481
 21. Li J Y, You B, Ding L, Xu J Z, Li W H, Chen H N, Gao H B. A novel bilateral haptic teleoperation approach for hexapod robot walking and manipulating with legs. *Robotics and Autonomous Systems*, 2018, 108: 1–12
 22. Bayle B, Fourquet J Y, Renaud M. Manipulability of wheeled mobile manipulators: application to motion generation. *The International Journal of Robotics Research*, 2003, 22(7–8): 565–581
 23. Peng J Z, Yu J, Wang J. Robust adaptive tracking control for nonholonomic mobile manipulator with uncertainties. *ISA Transactions*, 2014, 53(4): 1035–1043
 24. Wang Z P, Ge S S, Lee T H. Robust motion/force control of uncertain holonomic/nonholonomic mechanical systems. *IEEE/ASME Transactions on Mechatronics*, 2004, 9(1): 118–123
 25. Li Z J, Ge S S, Adams M, Wijesoma W S. Adaptive robust output-feedback motion/force control of electrically driven nonholonomic mobile manipulators. *IEEE Transactions on Control Systems Technology*, 2008, 16(6): 1308–1315
 26. Buchanan R, Bandyopadhyay T, Bjelonic M, Wellhausen L, Hutter M, Kottege N. Walking posture adaptation for legged robot navigation in confined spaces. *IEEE Robotics and Automation Letters*, 2019, 4(2): 2148–2155
 27. Tennakoon E, Peynot T, Roberts J, Kottege N. Probe-before-step walking strategy for multi-legged robots on terrain with risk of collapse. In: *Proceedings of 2020 IEEE International Conference on Robotics and Automation (ICRA)*. Paris: IEEE, 2020, 5530–5536
 28. Li K J, Ding X L, Ceccarelli M. A total torque index for dynamic performance evaluation of a radial symmetric six-legged robot. *Frontiers of Mechanical Engineering*, 2012, 7(2): 219–230
 29. Xu K, Ding X L. Gait analysis of a radial symmetrical hexapod robot based on parallel mechanisms. *Chinese Journal of Mechanical Engineering*, 2014, 27(5): 867–879
 30. Rosheim M E. *Robot Evolution: The Development of Anthropotics*. Hoboken: John Wiley & Sons, 1994
 31. Fang C. Motion planning and skill transfer of anthropomorphic arms based on movement primitives. Dissertation for the Doctoral Degree. Beijing: Beihang University, 2013 (in Chinese)
 32. Murray R M, Li Z X, Sastry S S. *A Mathematical Introduction to Robotic Manipulation*. Boca Raton: CRC Press, 2017
 33. Huang Z, Zhao Y S, Zhao T S. *Advanced Spatial Mechanism*. Beijing: Higher Education Press, 2006 (in Chinese)
 34. Zheng Y, Ding X L, Xu K. A novel six wheel-legged robot: structure design and stability analysis in different typical gaits. In: *Proceedings of the 14th IFToMM World Congress*. Taipei: Taiwan University, 2015, 296–304